



HAL
open science

On the combination of the planktonic foraminiferal Mg/Ca, clumped ($\Delta 47$) and conventional ($\delta 18\text{O}$) stable isotope paleothermometers in palaeoceanographic studies

Marion Peral, Franck Bassinot, Mathieu Daëron, Dominique Blamart, Jérôme Bonnin, Frans Jorissen, Catherine Kissel, Elisabeth Michel, Claire Waelbroeck, Helene Rebaubier, et al.

► To cite this version:

Marion Peral, Franck Bassinot, Mathieu Daëron, Dominique Blamart, Jérôme Bonnin, et al.. On the combination of the planktonic foraminiferal Mg/Ca, clumped ($\Delta 47$) and conventional ($\delta 18\text{O}$) stable isotope paleothermometers in palaeoceanographic studies. *Geochimica et Cosmochimica Acta*, 2022, 339, pp.22-34. 10.1016/j.gca.2022.10.030 . hal-04291869

HAL Id: hal-04291869

<https://hal.science/hal-04291869>

Submitted on 17 Nov 2023

HAL is a multi-disciplinary open access archive for the deposit and dissemination of scientific research documents, whether they are published or not. The documents may come from teaching and research institutions in France or abroad, or from public or private research centers.

L'archive ouverte pluridisciplinaire **HAL**, est destinée au dépôt et à la diffusion de documents scientifiques de niveau recherche, publiés ou non, émanant des établissements d'enseignement et de recherche français ou étrangers, des laboratoires publics ou privés.

Public Domain

1 **On the combination of the planktonic foraminiferal Mg/Ca, clumped (Δ_{47}) and**
2 **conventional ($\delta^{18}\text{O}$) stable isotope paleothermometers in palaeoceanographic studies**

3
4 Marion Peral^{1,2}, Franck Bassinot¹, Mathieu Daëron¹, Dominique Blamart¹, Jérôme Bonnin³,
5 Frans Jorissen⁴, Catherine Kissel¹, Elisabeth Michel¹, Claire Waelbroeck⁵, Helene
6 Rebaubier¹ and William R Gray¹

7
8 (1) Laboratoire des Sciences du Climat et de l'Environnement, LSCE/IPSL, CEA-CNRS-UVSQ, Université
9 Paris-Saclay, France

10 (2) Now at Analytical-Environmental and Geo-Chemistry, Vrije Universiteit Brussel, Belgium

11 (3) Université de Bordeaux, CNRS, Environnements et Paléoenvironnements Océaniques et
12 Continentaux (EPOC), UMR 5805, Allée Geoffroy St Hilaire, 33615 Pessac Cedex, France

13 (4) UMR CNRS 6112 LPG-BIAF Bio-Indicateurs Actuels et Fossiles, Université d'Angers, 2, Boulevard
14 Lavoisier, 49045 Angers Cedex, Franc

15 (5) LOCEAN/IPSL, Sorbonne Université-CNRS-IRD-MNHN, UMR7159, Paris, France
16

17 **Abstract**

18
19 Assuming that foraminiferal clumped isotope (Δ_{47}) values are independent of seawater salinity
20 and pH, the combination of Mg/Ca, $\delta^{18}\text{O}$ and Δ_{47} values, may in theory allow us to disentangle
21 the temperature, salinity/ $\delta^{18}\text{O}_{\text{sw}}$ and pH signals. Here, we present a new Mg/Ca- Δ_{47} dataset
22 for modern planktonic foraminifera, from various oceanographic basins and covering a large
23 range of temperatures (from 0.2 to 25.4 °C). These measurements were performed on the
24 same samples and species as the ones used for the foraminiferal Δ_{47} calibration of Peral et al.
25 (2018), allowing comparison between both Mg/Ca and Δ_{47} paleothermometers (excluding the
26 two benthic foraminiferal data points). There is a good agreement between these two
27 paleothermometers when the Mg/Ca-temperature is corrected for seawater salinity and pH,
28 suggesting that foraminiferal Δ_{47} may not be influenced by salinity or pH. However, our results
29 show that Δ_{47} temperature uncertainties still limit our ability to reconstruct pH and $\delta^{18}\text{O}_{\text{sw}}$
30 from the combination of Mg/Ca, $\delta^{18}\text{O}$ and Δ_{47} in a useful manner. We also find that
31 disagreements between Mg/Ca and Δ_{47} values in *G. bulloides* persist after correction for vital,
32 salinity and pH effects, suggesting that other process(es) may also influence Mg/Ca in this
33 species.

34 This study also provides an updated I-CDES version of the previously published planktonic and
35 benthic foraminiferal Δ_{47} calibration of Peral et al. (2018) , covering a range of temperature
36 from -2 to 25.4 °C.

37

38 1. INTRODUCTION

39

40 The reconstruction of key physical and chemical ocean water parameters, like
41 seawater temperature, salinity and pH, is critical to understand the processes driving past
42 ocean and climate variations. However, precisely quantifying these parameters remains
43 extremely challenging. Several proxies have been developed to reconstruct paleo-
44 temperatures, but they all suffer from various limitations and biases. In his seminal work on
45 isotopes, Harold Urey suggested that the extent by which ^{18}O was enriched in marine calcium
46 carbonates relative to the water from which it is precipitated, could be used as a past ocean
47 thermometer (Urey, 1947). However, later studies showed that this paleo-thermometer is
48 biased by the isotopic composition of the global ocean ($\delta^{18}\text{O}_{\text{sw}}$) that does not remain constant
49 but reflects the waxing and waning of large continental ice sheets over glacial and interglacial
50 cycles. This signal associated with global changes in continental ice volume strongly imprints
51 paleo- $\delta^{18}\text{O}$ records obtained from marine carbonates (Shackleton, 1967), with additional
52 contributions from regional modifications of evaporation/precipitation to a lesser degree.
53 Thus, it is impossible to accurately reconstruct past ocean temperature using the carbonate
54 $\delta^{18}\text{O}$ -thermometer without an independent knowledge of seawater $\delta^{18}\text{O}_{\text{sw}}$. Furthermore,
55 interspecies differences in the $\delta^{18}\text{O}$ -temperature relationship testify to the importance of
56 physiological processes, also called “vital” effects (e.g. Urey et al., 1951). In order to take into
57 account these effects, several authors developed species-specific calibrations (e.g., Bemis et
58 al., 1998; Mulitza et al., 2003).

59 More recently, several studies showed that the Mg/Ca elemental ratio of foraminiferal
60 calcite can be used to reconstruct paleo-seawater temperatures (Rosenthal et al., 1997; Lea
61 et al., 1999; Elderfield and Ganseen, 2000). Most foraminiferal species build their shells from
62 magnesium-poor calcite, in which the minor amount of Mg that can be substituted to Ca is
63 temperature dependent (Oomori et al., 1987). The paleoclimatology community had great
64 expectations regarding the combination of foraminiferal $\delta^{18}\text{O}$ and the Mg/Ca-thermometer,
65 which could be measured from the same material allowing theoretically to disentangle
66 temperature and $\delta^{18}\text{O}_{\text{sw}}$ signals. However, the Mg/Ca-thermometry proved to be more
67 complex and challenging than originally expected. First, it appeared that the partitioning
68 coefficient between Mg in seawater and Mg in the crystal matrix is not only

69 thermodynamically controlled by temperature, but also reflects physiological or ecological
70 processes (Rosenthal et al., 1997; Lea et al., 1999; Elderfield and Ganseken, 2000; Lea, 2014),
71 prompting several authors to develop species-specific, empirical Mg/Ca-temperature
72 calibrations (Nürnberg et al., 1996; Rosenthal et al., 1997; Lea et al., 1999; Erez, 2003). From
73 the first development of the Mg/Ca paleothermometer it was shown that foraminiferal Mg/Ca
74 is influenced by physico-chemical variables other than temperature such as bottom-water
75 carbonate ion concentration (Elderfield et al., 2006; Rosenthal et al., 2006), as well as surface
76 salinity (Nürnberg et al., 1996; Lea et al., 1999; Kısakürek et al., 2008; Mathien-Blard and
77 Bassinot; 2009, Gray et al., 2018; Gray and Evans, 2019) and pH (Lea et al., 1999; Gray et al.,
78 2018; Gray and Evans 2019), and - on time-scales longer than ~1 Ma - the Mg/Ca ratio of
79 seawater (Evans et al, 2016). In addition, analytical procedures must be carefully considered
80 since cleaning protocols have an effect on the measurement of Mg/Ca within foraminiferal
81 shells (Barker et al 2003; Pang et al., 2020 and references therein). These secondary influences
82 on foraminiferal Mg/Ca complicate its use as a temperature proxy.

83 The carbonate clumped isotope method (noted Δ_{47} hereafter) is one of the most recent
84 paleothermometers, which has been developed over the last decade (Eiler, 2007, 2011). The
85 Δ_{47} approach is based on the quantification of subtle statistical anomalies in the abundance
86 of doubly substituted carbonate isotopologues ($^{13}\text{C}^{18}\text{O}^{16}\text{O}^{16}\text{O}^{2-}$) relative to the random
87 distribution of isotopes (Eiler, 2007, 2011). A slightly higher abundance of $^{13}\text{C}^{18}\text{O}$ bonds is, for
88 thermodynamical reasons, a function of temperature (Eiler, 2011; Passey and Henkes, 2012;
89 Stolper and Eiler, 2016) and this relationship is independent of the $\delta^{18}\text{O}$ of water in which the
90 calcification occurs (Schauble et al., 2006). Clumped isotope methodological studies have
91 shown no evidence of vital effects (Tripathi et al., 2010; Grauel et al., 2013; Peral et al., 2018;
92 Piasecki et al., 2019; Meinicke et al., 2020) nor salinity effects (Grauel et al., 2013; Peral et al.,
93 2018) on foraminiferal Δ_{47} . Moreover, studies dealing with non-foraminiferal carbonates
94 (Tripathi et al., 2015; Watkins and Hunt, 2015) showed a lack of pH effect (or its negligible
95 influence) on clumped isotope. The absence of major biases would make Δ_{47} one of the most
96 promising paleo-thermometers. However, its use is still limited because of its low temperature
97 sensitivity and the large sample size required to significantly reduce the analytical
98 uncertainties. Obtaining precise and high-resolution Δ_{47} records remain a challenge.

99 Because of non-thermal effects on Mg/Ca from foraminifer shells, recent comparisons
100 revealed discrepancies between Mg/Ca- and Δ_{47} -derived temperatures (Peral et al., 2020;
101 Leutert et al., 2020; Meinecke et al., 2021). These discrepancies are not linked to any specific
102 foraminifer species (different species were used in the three studies), nor are they associated
103 to a given oceanic basin (samples from three different regions were studied, the
104 Mediterranean Sea, the Southern Ocean, and the Indian Ocean) or to a time period (the
105 studies covered from the late Pleistocene to 5 million years ago). We believe that these
106 discrepancies can be extremely informative as they may chiefly reflect vital effects and the
107 impact of salinity and pH on the Mg/Ca-thermometer, offering theoretically the opportunity
108 to disentangle temperature, salinity, and pH from the combination of $\delta^{18}\text{O}$, Mg/Ca and Δ_{47} in
109 planktonic foraminifera. Planktonic foraminiferal $\delta^{18}\text{O}$ depends on temperature and $\delta^{18}\text{O}_{\text{sw}}$,
110 the latter being correlated with the salinity. Carbonate $\delta^{18}\text{O}$ may be combined with Δ_{47} -
111 derived temperature to reconstruct the $\delta^{18}\text{O}_{\text{sw}}$ (Peral et al., 2020). As Mg/Ca is influenced by
112 salinity and pH, pH may be obtained by paring the Mg/Ca ratio with the reconstructed
113 temperature from Δ_{47} and salinity estimates from sea-level or from the combination of $\delta^{18}\text{O}$ -
114 Δ_{47} , following the equations described in Gray et al. (2018 and 2019). Combining $\delta^{18}\text{O}$, Mg/Ca
115 and Δ_{47} in foraminifera may therefore prove highly useful in palaeoceanographic studies.

116 The relationship between Mg/Ca and Δ_{47} in modern planktonic foraminifera has been
117 previously studied to investigate our ability to detect the potential biases associated to Fe-Mn
118 oxide coatings, contamination and/or dissolution of foraminiferal tests (Breitenbach et al.,
119 2018) in order to extract the best paleo-temperature estimates from non-biased
120 measurements. However, the sensitivity of foraminiferal Δ_{47} to salinity and pH has not been
121 given much attention so far and still needs to be examined since a potential dependence of
122 Δ_{47} on these chemo-physical parameters would potentially explain part of the differences
123 observed between the Δ_{47} and the Mg/Ca paleothermometers.

124 For the present paper, we measured Mg/Ca on the same set of samples and
125 foraminiferal species used in the Δ_{47} calibration of Peral et al. (2018). These data make it
126 possible to explore the sensitivity of foraminiferal Δ_{47} to salinity and pH and evaluate the
127 potential interest and limits of combining $\delta^{18}\text{O}$, Mg/Ca- and clumped-temperatures to
128 disentangle temperature, salinity- $\delta^{18}\text{O}_{\text{sw}}$, and pH effects. In the process, we took advantage
129 of re-calibrated clumped isotope data following cutting-edge methodological developments

130 to provide a revised version of the planktonic and benthic foraminiferal clumped isotope
131 calibration of Peral et al. (2018), that could be used for future paleoceanographic studies.

132

133 **2. MATERIALS AND METHODS**

134

135 **2.1. Samples**

136

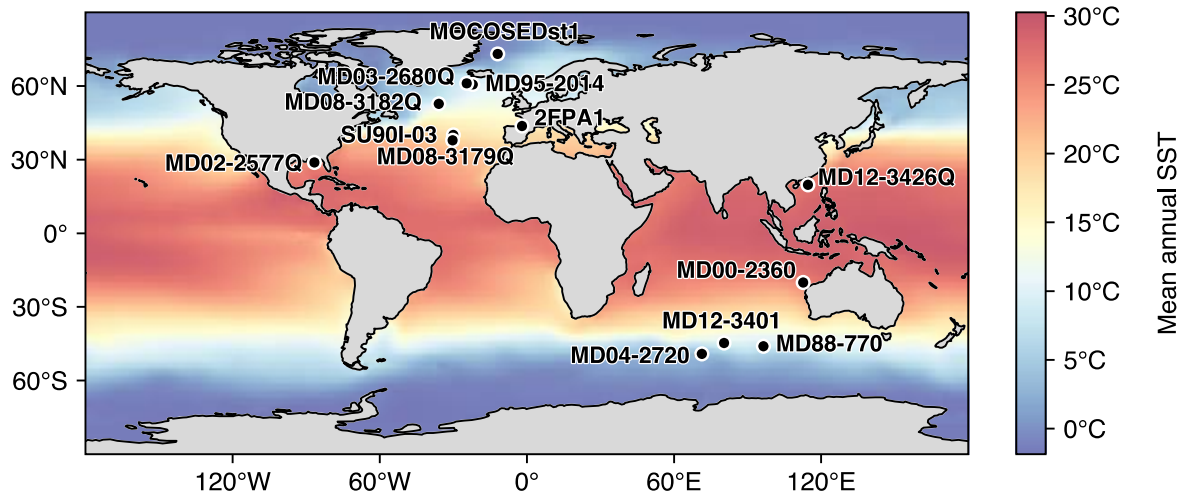
137 We used the same samples as those used in Peral et al. (2018), which are core-tops from
138 twelve marine sedimentary cores from different oceanographic basins in the North Atlantic,
139 Southern, Indian and Pacific Oceans (Fig. 1). All core-tops were chronologically constrained
140 and are from the late Holocene (Peral et al., 2018). The location of samples, the water depths
141 of the cores, the studied species and the ages are given in Table 1. We assume no changes in
142 temperature, salinity, and pH over the late Holocene at our core sites and use modern
143 hydrological atlases to estimate these data, at the location of our sites and at the living depths
144 of the planktonic species studied here (see paragraph 2.4.). As discussed later, the recent
145 warming and the addition of anthropogenic CO₂ to the surface ocean likely complicate the
146 comparison of instrumental carbonate system measurements with core-top foraminiferal
147 samples.

148 The core sites cover a wide range of seawater physico-chemical conditions, with
149 temperatures ranging from 0.2 to 25 °C (for the planktonic only) and from -2 to 25 °C (including
150 the benthic foraminifera), and with salinity ranging from 33.7 to 36.2 and pH from 7.7 to 8.1
151 (both for planktonic only). The top 1 cm of each sediment core-top was collected and dried
152 overnight at 50°C. The samples were wet sieved to collect the size fraction larger than 150 µm,
153 and the residues were dried. To limit the potential size effects on Mg/Ca, we picked the
154 planktonic foraminifera in narrow size ranges centered around the optimal size of each species
155 (i.e., the size corresponding to the maximum abundance of adult shells). The optimal sizes are
156 divided every ~50 µm (e.g., 200-250, 250-315, 315-355, 355-400, 400-450 and 450-500 µm).
157 Each species have their size ranges (see details in Table 2).

158 Nine species of planktonic foraminifera and two species of benthic foraminifera were
159 hand-picked under a binocular. For the Mg/Ca- Δ_{47} comparison, because of the differing
160 carbonate chemistry controls on Mg/Ca in planktonic and benthic foraminifera (Lea, 1999;
161 Elderfield et al 2006) we exclude the two benthic samples and only provide and discuss Mg/Ca

162 data from the planktonic foraminifera samples at the optimal size fractions. For the clumped-
163 isotope calibration, we include the benthic foraminifera data, and a large range of size as was
164 originally done in Peral et al. (2018).

165



166

167 **Figure 1:** Map showing the location of core-tops used in this study, with the mean annual SST
168 from WOA13

169

170 2.2. Clumped isotopes

171

172 The clumped-isotope data were previously published in Peral et al. (2018). The
173 methodology (from the cleaning protocol to the measurement) is described in Daëron et al.
174 (2016) and Peral et al. (2018). A summary of the cleaning protocol steps is presented in the
175 supplementary material (Fig. S1). In the present paper, we reprocessed our Δ_{47} data in
176 accordance with the new InterCarb - Carbon Dioxide Equilibrium Scale (I-CDES) and the
177 associated data processing methods (Bernasconi et al., 2021; Daëron, 2021).

178

179 In previous studies, discrepancies between clumped isotope calibrations had been
180 observed (e.g., Tripathi et al., 2010; Grauel et al., 2013). Thanks to an international effort,
181 several laboratories conducted an intercalibration exercise in order to determine clumped
182 isotope values of carbonate standards (ETH 1-4, IAEA-C1&2 and MERK; Bernasconi et al.,
183 2021). This new standardization approach (I-CDES reference frame) results in internationally
agreed calibrations (Anderson et al, 2021; Fiebig et al., 2021).

184 The Δ_{47} values of our modern foraminifera (Peral et al., 2018) were normalized to the
185 I-CDES reference frame (Bernasconi et al., 2021) using the carbonate standards ETH-1/2/3/4.
186 Data processing was performed using the Δ_{47} crunch library and the new pooled
187 standardization approach, as described in Daëron (2021). The reprocessed Δ_{47} calibration is
188 now compared with the new and/or other recalculated calibrations and used for future
189 paleoceanographic studies. The full dataset is provided in the supplementary material (Table
190 S1).

191 The Δ_{47} values were converted to temperatures using the Peral et al. re-calculated
192 calibration. The temperature uncertainties were estimated by propagating (i) the external
193 Δ_{47} reproducibility of our analytical sessions of measurements, based on repeated analyses of
194 standards and samples and (ii) the uncertainties associated with respective calibrations.
195 Recently, Anderson et al. (2021) have shown that when using the same standardization and
196 data processing, re-evaluated Δ_{47} -temperature calibrations obtained on various carbonate
197 materials agree within the range of uncertainty. In terms of Δ_{47} -temperature reconstructions,
198 using Peral et al. (2018) re-calculated calibration (this paper), or using the unified calibration
199 from Anderson et al. (2021), yield the same results. We found it important to provide in the
200 present paper a revised calibration equation that is based on cutting-edge approaches of Δ_{47}
201 standardization and processing methods (Bernasconi et al. 2021; Daëron, 2021) to serve for
202 future studies based on the state-of-the-art standard values.

203

204 **2.3. Mg/Ca analyses and derived temperatures**

205

206 **2.3.1. Mg/Ca measurements**

207

208 A total of 93 Mg/Ca analyses on 9 species of planktonic foraminifera were performed
209 at the Laboratoire des Sciences du Climat et de l'Environnement (LSCE) using a PlasmaQuant
210 ELITE Inductively coupled plasma mass spectrometry (ICP-MS) from Analytik Jena. One
211 milligram of foraminiferal shells was hand-picked for each sample allowing to perform 3 to 4
212 replicate analyses. We followed the cleaning protocol of Barker et al. (2003). Shells were
213 crushed between two glass plates and the resulting fragments were put into acid-leached
214 micro-vials. Fine material (i.e. clay) was removed through repeated ultrasonic cleaning with
215 18.2 M Ω water and then ethanol. In order to remove potential organic contaminants, the

216 samples were then oxidized with alkali-buffered 1% H₂O₂ solution for 10 minutes at 100°C.
217 The final cleaning treatment consists in a rapid leaching with 0.001 M HNO₃, before dissolution
218 in 0.15 M HNO₃. Samples are centrifuged immediately after dissolution and transferred to a
219 new acid-leached centrifuge tube, leaving a residual ~ 10 µl, which helps exclude any
220 remaining undissolved contaminants. Trace metal grade (NORMATOM) acids are used
221 throughout.

222 A 10 µl aliquot of each sample was first analyzed in order to determine calcium
223 concentrations. The samples were then diluted to a calcium concentration of 1mM Ca, to
224 match that of the bracketing standards. Mg/Ca ratios were measured using a modified version
225 of the method of Yu et al. (2005) against in-house standards prepared from single elementary
226 solutions. Mg/Ca instrumental precision was determined based on multiple replicates of a
227 standard solution of known Mg/Ca composition, with a long-term precision of 2% (2RSD).
228 Analysis of external standard NIST RM 8301 (Foraminifera) using our method gives a value of
229 2.65 ± 0.02 (1SE), in excellent agreement with its published value of 2.62 ± 0.14 (Stewart et
230 al., 2020). The data are summarized in Table 2 and the full data set is provided in
231 supplementary material (Table S2).

232

233 **2.3.2.** Correction of Mg/Ca for the effects of salinity and pH

234

235 We corrected our Mg/Ca values for pH and salinity effects based on the following
236 procedure: 1) using species-dependent calibrations, we calculated at each core location the
237 Mg/Ca values which are expected given the atlases-derived pH and salinity, and the $\delta^{18}\text{O}$ -
238 derived temperature, 2) at all the sites, we also calculated a pH- and salinity- normalized
239 Mg/Ca values (Mg/Ca normalized) by setting pH=8 and salinity=35, and using the sample-
240 specific oxygen isotopic-derived temperature; 3) the difference between the expected and
241 normalized Mg/Ca values provide correction values at each site and for each species, (4) these
242 correction values are then subtracted from our measured Mg/Ca values to cancel out the
243 salinity and pH effects from our data, thus leaving only temperature as a control parameter.

244

245 Practically, for the first step of this procedure, we used the species-specific equations
246 (Table 3) from Gray and Evans (2019) for *Globigerinoides ruber* and *Globigerina bulloides* to
247 estimate the “expected” Mg/Ca values. For the species for which a specific calibration is not

248 available, we used the generic equation of Gray and Evans (2019). To the best of our
249 knowledge, *N. pachyderma* is not pH sensitive (Tierney et al., 2019). Thus, no pH correction
250 was applied to the Mg/Ca of this species, and it is corrected for salinity only.

251 The multi-parameter regression equations of Gray and Evans (2019) provide Mg/Ca as
252 a function of the temperature, the salinity, and the pH of the sea water in which the
253 foraminifera have grown:

$$254 \quad \text{Mg/Ca} = \exp (a \times (S - a) + c \times T + d \times (\text{pH} - e)) + f$$

255 Where a, b, c, d, e and f are constants, and T, S and pH are the temperature (in °C), the salinity
256 and the pH of seawater during calcification. As said above, for each site and each species, we
257 solved the regression equations using modern, atlas-derived pH and salinities, and the
258 foraminifer $\delta^{18}\text{O}$ -derived temperature (see details in section 2.4), and then proceed to steps
259 2 to 4 (see above).

260

261

262 **2.3.3. Mg/Ca-derived temperatures**

263

264 **2.3.3.1 Multi-species calibration equation from Anand et al. (2003)**

265

266 In order to compare Mg/Ca and clumped-isotope-derived temperatures, we first
267 calculated the Mg/Ca-derived temperatures using the multi-species calibration of Anand et al.
268 (2003) solved using our pH- and salinity- corrected Mg/Ca values. The estimated-Mg/Ca
269 temperatures show a large difference when compared with the clumped-isotope-derived
270 temperatures (see supplementary material, Fig. S2). We recalculated the multi-species Anand
271 et al. (2003) calibration using the temperatures from the oxygen isotopic calibration of Kim
272 and O'Neil (1997). This equation may provide a more robust basis for reconstructing
273 temperature effects (Roche et al., 2018) than the modified, benthic-derived equation of
274 Shackleton (1974) originally used in the Anand et al. (2003) study (see details in section 2.4.1).
275 Following the same strategy as Anand et al. (2003), we only included the data from the 350 –
276 500 μm size-range and excluded the data from *Orbulina universa* and *Globigerinella*. We note
277 that, as shown in Anand et al. (2003), the measured $\delta^{18}\text{O}_{\text{calcite}}$ is up to ~ 1 per mil too light in
278 the wintertime compared to the value predicted using the measured sea surface temperature-
279 and salinity-based $\delta^{18}\text{O}_{\text{sw}}$ estimates at the Sargasso Sea sediment trap site. This is likely due to

280 a seasonal change in the $\delta^{18}\text{O}_{\text{sw}}$ -salinity relationship at this site, which potentially introduces
281 a substantial bias to the resulting Mg/Ca equation (Gray et al, 2018). The recalculated equation
282 is presented in Table 3 and shown in supplementary material (Data Processing file).

283

284 2.3.3.2 Mono species-specific equations

285

286 We first used calibration equations that were derived by linking Mg/Ca to temperature
287 only. To the best of our knowledge, we chose the most adequate calibrations, considering the
288 species, the size fraction, the oceanic region, and the cleaning protocol. For seven of the
289 planktonic species studied in the present manuscript, we used the mono-specific equations of
290 Anand et al. (2003). Unfortunately, the only available calibration for *Globorotalia menardii*
291 was established using a cleaning protocol with a reductive step (Regenberg et al., 2010), which
292 is known to lower the Mg/Ca ratio of foraminifera compared to the cleaning approach of
293 Barker et al. (2003) that we used for the present paper (e.g., Pang et al., 2020). In the absence
294 of a calibration for *Neogloboquadrina pachyderma* (dextral), we used the same calibration as
295 the one developed for *N. pachyderma* (sinistral) (Vázquez Riveiros et al., 2016). The
296 uncertainties were calculated by propagating the analytical errors, based on the long-term
297 standard deviation of our standards and the uncertainties associated with the respective
298 calibrations.

299 It is important to underline that, for internal consistency, the mono-species calibrations were
300 corrected for local pH and salinity effects, as described in section 2.3.2. (i.e. species-specific
301 equation of Gray and Evans (2019) with isotopic temperature, and salinity and pH from the
302 atlases). For the Anand et al. (2003) calibrations, we used the *in situ* salinities available in
303 Deuser and Ross (1989). The calibration of Regenberg et al. (2010) based on *G. menardii* was
304 not corrected because we could not find the raw Mg/Ca data.

305

306 **2.4. Independent constraints on temperatures, salinity and pH from Δ_{47} and Mg/Ca ratios**

307

308 **2.4.1. Estimation of calcification temperatures**

309

310 In order to limit uncertainties associated to the imperfect knowledge of planktonic
311 foraminifera ecology, numerous authors have used $\delta^{18}\text{O}$ -derived temperatures instead of

312 atlas temperatures for the calibration of geochemical proxies (e.g. Anand et al., 2003;
313 Mathien-Blard and Bassinot, 2009; Peral et al., 2018; Meinicke et al., 2020). Comparing
314 WOA13 atlas temperatures and foraminifer $\delta^{18}\text{O}$ -derived temperatures obtained using
315 various calibration equations, Peral et al. (2018) suggested the use of the calibration equation
316 of Kim and O'Neil (1997), modified for consistency by using an acid fractionation factor
317 (difference of oxygen isotope ratio between the mineral (calcite) and the CO_2 gas evolved from
318 acidification with phosphoric acid) of 1.01025 (Eq. 1). The Kim and O'Neil (1997) calibration is
319 then used to calculate the $\delta^{18}\text{O}$ -derived temperatures in this study:

320

$$321 \quad 1000 \ln(\alpha_{\text{CC/W}}) = 18.03 \times 1000 / T - 32.17 \quad (\text{Eq. 1})$$

322

323 Where T is the isotopic temperature in Kelvin and $\alpha_{\text{CC/W}}$ is the oxygen-18 fractionation factor
324 between calcite and water, with:

325

$$326 \quad \alpha_{\text{CC/W}} = (1 + \delta^{18}\text{O}_{\text{C/SMOW}} / 1000) / (1 + \delta^{18}\text{O}_{\text{SW/SMOW}} / 1000) \quad (\text{Eq. 2})$$

327

328 Where $\delta^{18}\text{O}_{\text{C/SMOW}}$ and $\delta^{18}\text{O}_{\text{SW/SMOW}}$ correspond to foraminiferal calcite and seawater $\delta^{18}\text{O}$
329 relative to VSMOW. Following the recommendation of Marchitto et al. (2014), $\delta^{18}\text{O}_{\text{C}}$ values
330 for *Uvigerina* were adjusted by subtracting 0.47 ‰.

331 Seawater $\delta^{18}\text{O}$ values at each core site were extracted from the gridded data set of
332 LeGrande and Schmidt (2006). The same approach as the WOA-temperature extraction is
333 followed (as described in Peral et al., 2018). Because one still does not know well the exact
334 habitat depth and growth season of planktonic species and their spatial variability in relation
335 to nutrient availability and physico-chemical conditions (i.e., Retailleau et al., 2011; Schiebel
336 and Hemleben, 2017), we followed the same approach as Peral et al. (2018). We calculated
337 the $\delta^{18}\text{O}_{\text{SW}}$ of seawater in which foraminifera calcified by averaging at each site the gridded
338 $\delta^{18}\text{O}_{\text{SW}}$ of LeGrande and Schmidt (2006) over species-specific living depth ranges. These depth
339 ranges may vary across ocean basins. According to Tolderlund and Be' (1971) and Durazzi
340 (1981), living depths in the North Atlantic Ocean range between 0 – 50 m for *G. ruber* and *O.*
341 *universa*, and the depth range is 0-100m for *G. bulloides*, *G. truncatulinoides*, *G. menardii* and
342 *G. inflata* (Steinke et al., 2005; Numberger et al., 2009, Rebotim et al 2017). For *N.*

343 *pachyderma*, the living depth is estimated from 0 to 200 m depth (Rebotim et al., 2017). In the
344 Indian Ocean, Duplessy et al. (1981) placed the depth of calcification for all these species
345 within and below the mixed layer, except for *G. ruber* and *G. menardii* which are believed to
346 remain respectively at the surface and within the mixed layer (0–100 m). In the South China
347 Sea, *G. ruber* and *G. menardii* are described as living near the surface and in the top 100 m,
348 respectively (Pflaumann and Jian, 1999). Finally, the living depth of *O. universa* being very
349 poorly constrained to the best of our knowledge, we assume that it lives everywhere at the
350 same depth as in the North Atlantic Ocean (Rebotim et al., 2017). For benthic foraminifera (re-
351 calibration of clumped isotope versus temperature), we must use the bottom $\delta^{18}\text{O}_{\text{SW}}$ values.
352 For the planktonic foraminifera, the mean $\delta^{18}\text{O}_{\text{SW}}$ values averaged for the living depth of each
353 species for each oceanic basin is considered. The uncertainty of $\delta^{18}\text{O}_{\text{SW}}$ at each site was
354 estimated as the quadratic sum of the site-specific standard deviation of $\delta^{18}\text{O}_{\text{SW}}$ within the
355 corresponding water depth and a constant error of 0.20 ‰ assigned to the GISS grid
356 interpolation. Final uncertainties of the oxygen isotopic temperatures are propagated based
357 on the $\delta^{18}\text{O}_{\text{SW}}$ uncertainties and the external analytical error on $\delta^{18}\text{O}$ values.

358 For *G. bulloides* and *O. universa*, we could also compare the reconstructed Mg/Ca-
359 temperatures to $\delta^{18}\text{O}$ -temperatures obtained using the species-specific $\delta^{18}\text{O}$ calibrations from
360 Bemis et al. (1998). This comparison is presented in Figure S3 and discussed in paragraph 4.2.

361

362 **2.4.2.** Estimation of seawater salinity and pH

363

364 The seawater salinity values at each core-top location were extracted from the WOA13
365 gridded data set (Zweng et al., 2013). As for the GISS $\delta^{18}\text{O}_{\text{SW}}$ values (see above), for each ocean
366 basin, we computed the seawater salinity in which the foraminifera calcified by averaging the
367 atlas salinities over the living depth range known for each species. Uncertainties were
368 estimated at each site as the quadratic sum of a nominal error of 0.20 arbitrarily assigned to
369 the WOA13 data set and the site-specific standard deviation of salinity.

370 The seawater pH values at each core-top location and for each species living depth
371 were extracted from the GLODAP 2020 data set (Olsen et al., 2020). Similarly, following the
372 same strategy as for the GISS $\delta^{18}\text{O}_{\text{SW}}$ and WOA13 salinity, we averaged the available GLODAP
373 2020 data over the living depth-range published for each species. A pH uncertainty of 0.02

374 was assigned to GLODAP pH data (Olsen et al., 2020). We note that this only represents a
375 'climatological' error. The use of climatological pH data is far from ideal because, due to the
376 release of anthropogenic CO₂, the surface ocean has acidified considerably since 1850. This
377 has lowered the pH relative to the pre-industrial value, whereas the vast majority of
378 foraminifera retrieved in the core top samples are likely to be of preindustrial age or older.
379 This pH uncertainty represents a major source of uncertainty in our analysis and is a major
380 hindrance to usefully constraining the sensitivity of foraminiferal proxies to the carbonate
381 system using coretop material.

382

383 **3. RESULTS**

384

385 **3.1. Clumped isotope dataset**

386

387 The clumped-isotope calibration using the same data set as Peral et al. (2018) is
388 recalculated following the latest methodological developments (see section 2.2 for details).
389 The recalculated clumped-isotope data range from 0.6976 ‰ to 0.5917 ‰ and cover a range
390 of temperatures from -2.3 to 25.4 °C (oxygen isotopic temperatures from eq. 1 are used in the
391 whole section; Table 2). As expected, the Δ_{47} values increase with decreasing temperatures;
392 the benthic foraminifera sample from the arctic (*C. wuellerstorfi* – MOCOSED-St1) shows the
393 highest Δ_{47} value, while planktonic foraminifer sample from one of the warmest sites *G. ruber*
394 – MD00-2360) shows the lowest Δ_{47} value.

395

396 **3.2. Raw Mg/Ca dataset**

397

398 We only measured Mg/Ca for the planktonic foraminifera. Our raw Mg/Ca dataset
399 ranges from 0.8 to 7.7 mmol/mol (Table 2 for the whole section) and covers a range of
400 temperatures from -0.7 to 25.4 °C (temperatures for the whole section; Table 2). As expected,
401 the cold-water dwelling foraminifera (*N. pachyderma* s. – MOCOSED st 1) show the lowest
402 Mg/Ca values and the warm-water surface dwellers such as *G. ruber* and *O. universa* show the
403 highest Mg/Ca values. Note the particularly high value (Mg/Ca =7.7 mmol/mol) obtained for
404 *O. universa* . This species likely calcifies at a lower temperature than *G. ruber*, which
405 nevertheless shows a raw Mg/Ca value of only 4.3 mmol/mol (sample of MD00-2360). Our

406 data therefore support previous observations that *O. universa* is characterized by unusually
407 high Mg/Ca ratios (Lea, 1999; Anand et al., 2003).

408 The raw Mg/Ca ratios measured on the same samples and species, but for different
409 size fractions, show a maximum difference of 0.4 mmol/mol between all the size fractions.

410

411 **3.3. Corrected Mg/Ca**

412

413 The raw Mg/Ca values are corrected for salinity and pH from atlas data, using the
414 method as described in section 2.3.2. The corrected Mg/Ca, excluding *N. pachyderma*
415 samples, ranges from 1.6 mmol/mol (Table 2) for *G. bulloides*-MD12-3401 that calcified at 5
416 °C (isotopic temperatures, Table 2), to 4.9 for *G. ruber*-MD00-2360 that calcified at 24.8 °C
417 (isotopic temperatures, Table 2). It is also noticeable that *G. bulloides* species still records high
418 Mg/Ca values, as discussed in part 4.3. For a better comparison between our Δ_{47} and Mg/Ca
419 values, we test all subsequent analysis with and without *G. bulloides* in the dataset. The
420 corrected Mg/Ca values for the species coming from the same core tops display a consistent
421 relationship with calcification temperatures.

422

423 **3.4. Comparison of Mg/Ca-derived temperatures (multi-species and mono-species 424 equations) with $\delta^{18}\text{O}$ and Δ_{47} -derived temperatures**

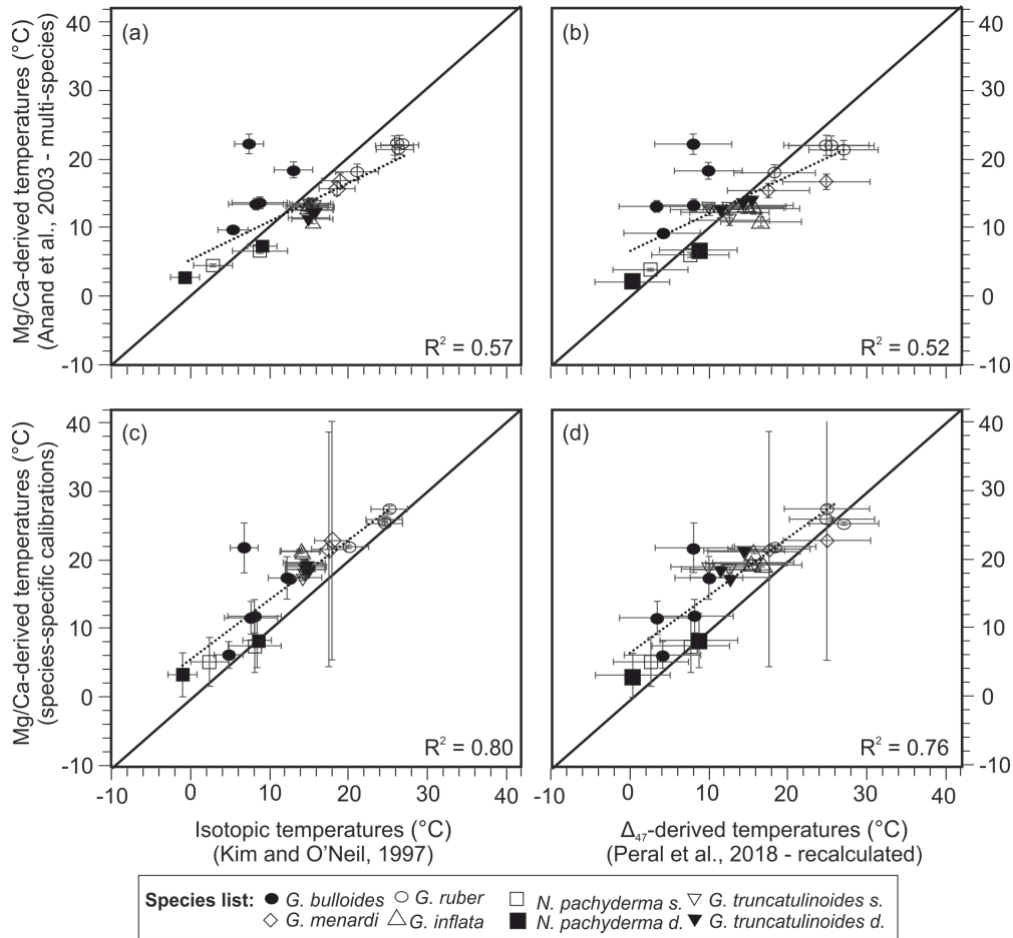
425

426 The Mg/Ca-derived temperatures were estimated using the recalculated multi-species
427 calibration of Anand et al. (2003) and compared to the $\delta^{18}\text{O}$ -temperatures (Fig. 2.a) estimated
428 using Kim and O'Neil (1997) equation (eq. 1), as described in section 2.4.1. The Mg/Ca-
429 temperatures for the species *G. bulloides* are systematically higher than the $\delta^{18}\text{O}$ -derived
430 temperatures, while most of the other species display lower Mg/Ca-derived temperatures
431 (Fig. 2.a). A linear regression only explains 57 % of co-variance between the two thermometers
432 (Fig. 2.a).

433 Then, the Mg/Ca-derived temperatures reconstructed using the multi-species
434 calibration of Anand et al. (2003) are compared to the Δ_{47} -derived temperatures obtained
435 using the recalculated version of the foraminifer calibration equation of Peral et al. (2018; see
436 section 2.3; Fig. 2.b). As was observed with the $\delta^{18}\text{O}$ -temperatures, the *G. bulloides* species

437 show higher Mg/Ca-derived temperatures than those derived from Δ_{47} and a linear regression
 438 only explains 52 % of co-variance between the two thermometers (Fig. 2.b).

439 We then computed Mg/Ca-derived temperatures using mono-species calibrations.
 440 These Mg/Ca-temperatures are in better agreement with $\delta^{18}\text{O}$ -derived temperatures (Table
 441 3; Fig. 2.c) and Δ_{47} -derived temperatures (Fig. 2.d.), with regression equations explaining 80 %
 442 and 76 % of co-variance. However, Mg/Ca-derived temperatures are always warmer than the
 443 isotopic temperatures.



444
 445 **Figure 2:** Comparison of temperature estimates obtained on 9 planktonic species. Top panels:
 446 reconstructed Mg/Ca temperatures using the recalculated multi-species calibration of Anand
 447 et al. (2003) compared to reconstructed $\delta^{18}\text{O}$ temperatures, using Kim and O'Neil (1997) (a)
 448 and Δ_{47} -derived temperatures, using the recalculated calibration equation of Peral et al.
 449 (2018) (this paper) (b). Bottom panel: reconstructed Mg/Ca derived temperatures using the
 450 most adequate mono-specific calibrations compared to reconstructed $\delta^{18}\text{O}$ temperatures,
 451 using Kim and O'Neil (1997) (c) and Δ_{47} -derived temperatures, using recalculated Peral et al.

452 (2018) calibration (d). Dotted black lines are linear regressions, the black solid lines are the 1:1
 453 line. Uncertainties are at 2SE.

454

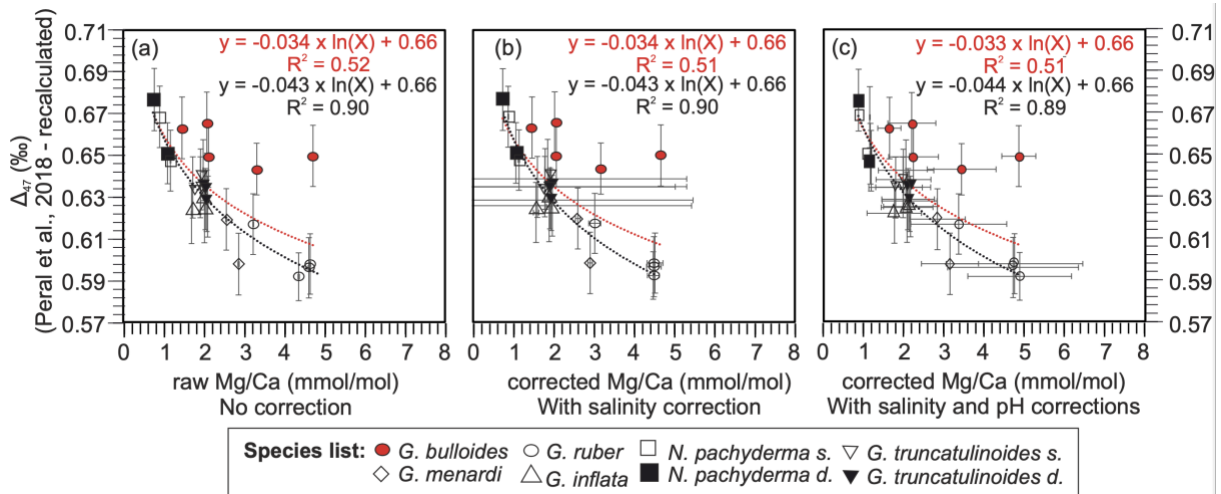
455 **3.5. Δ_{47} values versus raw, corrected Mg/Ca values**

456

457 The Δ_{47} values (recalculated from the raw data of Peral et al., 2018) are compared to
 458 (1) the raw Mg/Ca values (Fig. 3.a – without *O. universa*), (2) the Mg/Ca values corrected for
 459 seawater salinity only (i.e. setting d constant to zero in the correction equations from Gray
 460 and Evans, 2019) (Fig. 3.b), and (3) the Mg/Ca values corrected for both seawater salinity and
 461 pH salinity (Fig. 3.c).

462 The raw Mg/Ca data (without corrections) show a poor agreement with the Δ_{47} values
 463 (Fig. 3.a; $R^2 = 0.52$). Similarly, poor agreement is observed using either "salinity" corrected
 464 Mg/Ca or "salinity + pH" corrected Mg/Ca. " ($R^2 = 0.51$ in Fig. 3.b & c). However, it should be
 465 noted that without the *G. bulloides* samples, the agreements for the three comparisons
 466 improve significantly with an R^2 of 0.90, 0.90 and 0.89, respectively (Fig. 3.a&b&c).

467



468

469 **Figure 3:** Comparison of our recalculated foraminiferal Δ_{47} values with raw Mg/Ca values
 470 (uncorrected) (a), with corrected Mg/Ca for salinity only (b), and with corrected Mg/Ca for
 471 salinity and pH (c). The Mg/Ca values are corrected using the equations from Gray and Evans
 472 (2019), the salinity and pH from the atlas and the oxygen isotopic temperatures. The red
 473 dotted logarithmic regressions are plotted for all the plots, including *G. bulloides* and the black
 474 regressions are without *G. bulloides*. All the uncertainties are at 2SE.

475

476 **4. DISCUSSION**

477

478 **4.1. Updated foraminiferal clumped-isotope calibration**

479

480 The efforts of the clumped-isotope community have led to the establishment of an
481 international standardization and a uniform measurement data processing, allowing
482 robust/accurate comparisons between Δ_{47} measurements performed in different laboratories
483 (Bernasconi et al., 2021, and Fig. 4 therein). Following the newest methodological
484 advancements in clumped isotope – new standard values and data processing (see details in
485 section 3.2) - (Bernasconi et al., 2021; Daëron, 2021), we recomputed the multi-foraminiferal
486 species calibration from Peral et al. (2018) (Fig. 4). The total least squares regression yields the
487 following relationship:

488

$$489 \quad \Delta_{47} = A \times 10^3 / T^2 + B \quad \text{eq. 3}$$

490

491 Where $A = 37.0$ and $B = 0.181$

492 To compute the formal standard errors for this regression, we reformulate the
493 equation 3 in terms of the barycenter of our $(1/T^2_0)$ values, so that parameters A and B_0 are
494 statistically independent:

495

$$496 \quad \Delta_{47} = A*(T^{-2} - T_0^{-2}) + B_0 \quad \text{eq. 4}$$

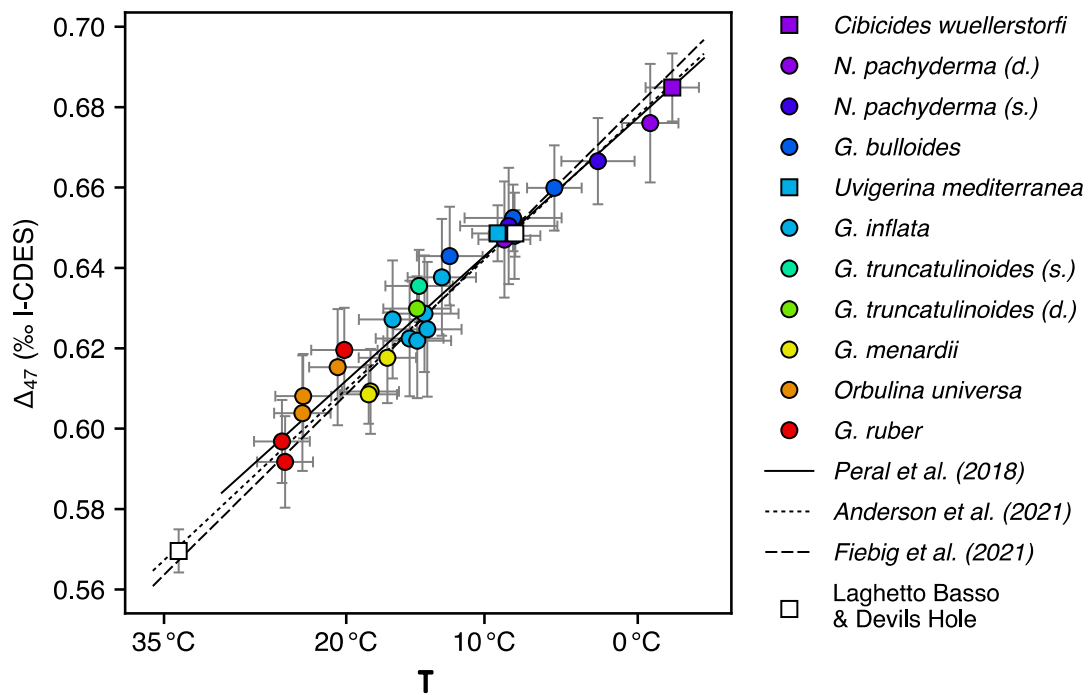
497

498 Where $A = 37.0$ (SE = 2.0), $B_0 = 0.636$ (SE = 0.0025) and $T_0 = 285.1$ K

499

500 The conclusions drawn by Peral et al. 2018) based on the original data, are still valid –
501 i.e. no apparent species-specific foraminiferal size and salinity effects (cf. Peral et al., 2018 for
502 more details). The updated calibration established in the present paper is compared with the
503 unified calibration of Anderson et al. (2021) and the precise inorganic calibration of Fiebig et
504 al. (2021) (Fig. 4). A good agreement (in the range of 0.3 – 1.3 °C, within the calibration
505 uncertainties) is observed between the three calibrations. This agreement between biogenic
506 carbonates (this study) and inorganic carbonates (Anderson et al., 2021; Fiebig et al., 2021 and
507 the slow-growing Laghetto Basso and Devils Hole calcite (Daëron et al., 2019; Anderson et al.,

508 2021)) confirms that using standardized protocols (Bernasconi et al., 2021; Daëron, 2021)
 509 solves the large discrepancy between the calibrations (Anderson et al., 2021; Fiebig et al.,
 510 2021). Also, this calibration constitutes the more precise equation based on foraminifera.
 511 These observations allow a direct application of this calibration to foraminifera for
 512 palaeoceanographic studies; this recalculated version of the calibration by Peral et al. (2018)
 513 should be used instead of the original version for future paleoceanographic studies.



514
 515 **Figure 4:** Recalculated Δ_{47} values (mean and 2SE) compared to oxygen isotopic temperatures
 516 (mean and 2SE) obtained with Kim and O’Neil (1997) for planktonic (circle) and benthic
 517 (square) foraminifera samples, combining all size fractions (modified from Peral et al., 2018).
 518 The new calibration regression corresponds to the black line (Peral et al., 2018 recalculated).
 519 The recalculated foraminiferal calibration is compared to the slow-growing calcite from
 520 Laghetto Basso and Devils Hole (from Anderson et al., 2021) and to calibrations of Anderson
 521 et al. (2021) and Fiebig et al. (2021)

522
 523 **4.2. Species specific effects on Mg/Ca-temperatures vs Δ_{47} -temperatures comparison**
 524

525 By comparing various paleothermometers we are able to better constrain the
526 limitations of each of the methods and, within the framework of these limitations, try to
527 extract as much meaningful climatic information as possible by combining those proxies.

528 The plot of Mg/Ca-temperatures vs Δ_{47} -derived temperatures (Fig. 2.b) shows a larger
529 scattering around the 1:1 line than the plot displaying Mg/Ca-temperatures vs $\delta^{18}\text{O}$ -derived
530 temperatures (Fig. 2.a). This larger scattering likely results from the higher uncertainties in the
531 clumped-isotope-derived temperatures. The use of species-specific calibrations for Mg/Ca-
532 derived temperatures improves the fit with the Δ_{47} -derived temperatures, compared to the
533 use of a multi-species calibration (Fig. 2.d vs Fig. 2.b). No species-specific calibration is
534 necessary for clumped isotope as Δ_{47} thermometer does not appear to be affected by species-
535 specific effects (Tripathi et al., 2010; Grauel et al., 2013; Peral et al., 2018; Meinicke et al., 2020).

536 Although R^2 values significantly increase when using species-specific Mg/Ca
537 calibrations, the Mg/Ca-derived temperatures are systematically warmer than $\delta^{18}\text{O}$ - and Δ_{47} -
538 derived temperatures (Fig. 2.b&d – linear regression lines). This is coherent with previous
539 observations (Peral et al., 2020; Leutert et al., 2020).

540 No significant improvement is observed when species-specific calibrations are used to
541 reconstruct temperatures from *G. bulloides* and *O. universa* $\delta^{18}\text{O}$ (Bemis et al., 1998) (Figure
542 S3). *G. bulloides* Mg/Ca data result in temperatures as high as 20 °C, showing up to 12 °C
543 difference with the two isotopic thermometers (see discussion below in section 4.3.). One
544 second explanation would be the dependance of Mg/Ca values on salinity and pH (Nürnberg
545 et al., 1996; Kısakürek et al., 2008; Mathien-Blard and Bassinot, 2009, Gray et al., 2018; Gray
546 and Evans, 2019). It has been shown that the Δ_{47} in foraminifera is not affected by salinity
547 (Tripathi et al., 2010; Peral et al., 2018), however, the pH dependence of the foraminiferal Δ_{47}
548 thermometer has never been studied to this date. By comparing both foraminiferal- Δ_{47} and
549 corrected-Mg/Ca temperatures, the potential effect of pH on clumped isotopes can be
550 deciphered.

551

552 **4.3. *G. bulloides* species in Mg/Ca**

553

554 The relatively poor correlation between raw or corrected Mg/Ca and clumped isotope
555 (Fig. 3a&b&c) chiefly results from particularly high *G. bulloides* Mg/Ca values and the high
556 variability of *G. bulloides* data over a narrow Δ_{47} range (Fig. 3a&b&c). The correlations

557 significantly improve when *G. bulloides* samples are excluded. The high Mg/Ca ratios
558 measured in *G. bulloides* and their important variability are not explained by anomalous, local
559 salinity or pH values. High *G. bulloides* Mg/Ca values could be likely explained by 1) diagenesis
560 or metal coating, 2) pH effect on $\delta^{18}\text{O}$ measurements or 3) the existence of different *G.*
561 *bulloides* morphotypes and/or genotypes characterize by different temperature-driven Mg/Ca
562 incorporation mechanisms.

563 1) Diagenesis or metal coating: The relationship between foraminiferal Δ_{47} and raw Mg/Ca
564 has been previously examined by Breitenbach et al. (2018). These authors suggested that the
565 clumped isotope-Mg/Ca comparison could help identify potential problems and biases of the
566 Mg/Ca-thermometer resulting from Fe-Mn oxide coatings, clay contamination and/or
567 foraminiferal test dissolution. Our foraminifera samples are in a good state of preservation
568 and do not suffer from dissolution (SEM pictures available in Peral et al., 2018). Additionally,
569 the Fe/Ca and Mn/Ca values are low in our dataset, below the thresholds that lead to suspect
570 a contamination problem (Boyle and Keigwin (1985); see supplementary material Table S2).
571 Nevertheless, the *G. bulloides* sample showing the highest Mg/Ca value (sample from core
572 MD95-2014) displays also an anomalously high Al/Ca content of 7337 mmol/mol compared to
573 the other samples for which Al/Ca values are below 100 mmol/mol. For this sample,
574 contamination by clay minerals is likely. Our observations suggest that the Fe-Mn oxide
575 coatings, clay contamination (except for one sample) and/or foraminiferal test dissolution do
576 not explain the too high Mg/Ca values of *G. bulloides* and the higher range of variability when
577 compared with Δ_{47} values.

578 2) pH effect on the $\delta^{18}\text{O}$ measurements: $\delta^{18}\text{O}$ -derived temperatures are used to correct
579 the Mg/Ca; but the $\delta^{18}\text{O}$ of *G. bulloides* may be affected by pH effect (Spero et al., 1997; Spero
580 et al., 1999; Zeebe, 1999). As a result, the high corrected Mg/Ca may be due to not considering
581 the pH effect on $\delta^{18}\text{O}$. However, if the Mg/Ca is corrected using the temperature from the
582 WOA rather than by the $\delta^{18}\text{O}$ -derived temperature, the conclusion is similar: high corrected
583 Mg/Ca is obtained. The pH effect on *G. bulloides* $\delta^{18}\text{O}$ cannot explain the high Mg/Ca ratio.

584 3) *G. bulloides* has been shown to present different morphotypes and also different
585 genotypes (sometimes with a similar morphotype), these cryptic species can potentially live at
586 different depths and have specific ecological niches (Osborne et al., 2020). The Δ_{47} values of
587 *G. bulloides* are in very good agreement with the other species used and do not show
588 systematic biases (Fig. 3), suggesting that the singularity of *G. bulloides* data in the Mg/Ca. vs.

589 Δ_{47} only occur in Mg/Ca ratio. The Δ_{47} SD of the *G. bulloides* measurements are good,
590 suggesting that in any given sample, *G. bulloides* with the same morphotype and/or genotype
591 were picked. However, we cannot exclude the possibility that different genotypes (with similar
592 morphotype) were analyzed at different sites. More detailed studies on *G. bulloides* are
593 essential to better understand the potential cryptic variability of this species and its impact on
594 Mg/Ca incorporation.

595 In the rest of the article, *G. bulloides* samples are removed from the dataset to better
596 compare the corrected Mg/Ca and the clumped isotope-derived temperatures.

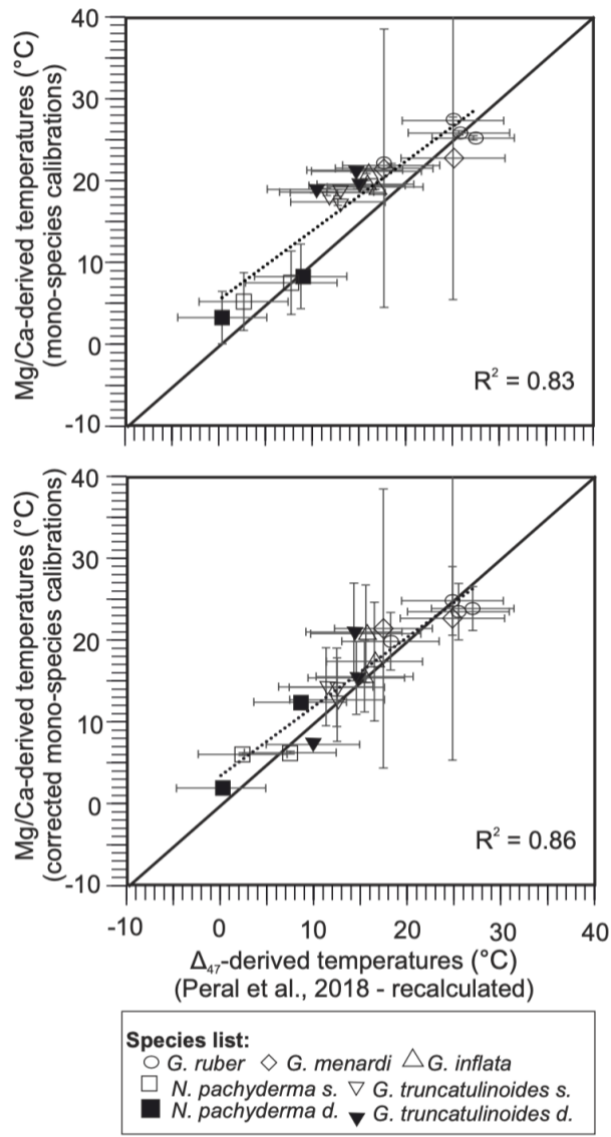
597

598 **4.4. Salinity and pH effects on reconstructed Mg/Ca vs Δ_{47} temperatures**

599

600 Considering that the Δ_{47} is independent of salinity and pH, and by correcting the Mg/Ca
601 temperatures for each of these parameters, the observations made on figure 2 may be
602 explained. In figure 5, we redraw the Mg/Ca-temperature vs. Δ_{47} -temperature comparison of
603 Figure 2d (i.e. obtained using the mono-specific calibration equations) but without *G.*
604 *bulloides*. The mono-species Mg/Ca calibrations are corrected for salinity and pH (section
605 2.3.3). Using this corrected-mono-species calibrations for Mg/Ca-derived temperature, the
606 comparison with Δ_{47} -derived temperatures is better; the regression line is close to the 1:1 line
607 and explains 86% of the co-variance between both thermometers (Fig. 5). Thus, our results
608 concur with observations from the geological record (Leutert et al, 2020; Meinecke et al 2021),
609 that improved agreement between Δ_{47} -derived and Mg/Ca-derived temperatures is observed
610 when the influences of pH and salinity on Mg/Ca are accounted. This emphasizes the
611 importance of correcting Mg/Ca values for non-thermal influences. However, it is noticeable
612 that cold Mg/Ca-derived temperatures still show a slight difference with Δ_{47} -derived
613 temperatures. This could result from the small number of samples available and/or specific
614 problems (e.g., effects of species, CO_3^{2-}). More data is requested on the cold end member to
615 better understand this potential difference.

616 The good agreement between the Δ_{47} -derived temperatures and corrected Mg/Ca-
617 derived temperatures provides further support that Δ_{47} is not affected by salinity (Tripathi et
618 al., 2010; Peral et al., 2018) and pH (or that the effect of pH is negligible).



619

620 **Figure 5:** Mg/Ca-derived temperatures using mono-species calibrations, compared to the Δ_{47} -
 621 derived temperatures using the recalculated Peral et al. (2018) calibration (a) and the Mg/Ca-
 622 derived temperatures using the corrected Mg/Ca mono-species calibrations for salinity and
 623 pH compared to the Δ_{47} -derived temperatures using the recalculated Peral et al. (2018)
 624 calibration (b). The dotted linear regression, excluding *O. universa* and *G. bulloides*, is plotted.
 625 A line 1:1 is plotted in black; uncertainties are at 2 SE.

626

627 4.5. The potential of combining Mg/Ca ratio, $\delta^{18}\text{O}$ and Δ_{47} for palaeoceanographic studies

628

629 The combination of $\delta^{18}\text{O}$ and Δ_{47} in foraminifera has been previously studied to
 630 accurately reconstruct the signal of $\delta^{18}\text{O}_{\text{sw}}$ even during glacial-interglacial scales (Rodriguez-
 631 Sanz et al., 2021; Peral et al., 2020). Next, the comparison between Mg/Ca and Δ_{47}

632 systematically shows differences between the two thermometers in modern and fossil
633 foraminifera. Breitenbach et al. (2018) showed that combining Mg/Ca and clumped isotopes
634 data may help to detect possible dissolution and metal coating biases on the Mg/Ca-
635 thermometer. When samples are not biased by contamination, dissolution or diagenesis, the
636 combination of these two proxies has been used to estimate long-term variations in seawater
637 Mg/Ca (Evans et al., 2018; Meinecke et al., 2021).

638 In the present study, we showed that salinity and pH lead to discrepancies between
639 clumped isotope and Mg/Ca in planktonic foraminifera frequently used for paleoceanographic
640 reconstructions (however, further work is needed for *O. universa* and *G. bulloides*). Because
641 of the multi-parameter dependency of foraminiferal $\delta^{18}\text{O}$, Δ_{47} and Mg/Ca, the combination of
642 these paleo-thermometers could provide us with more than just the estimates of past ocean
643 temperatures. Theoretically, based on the Gray and Evans equation (2019), the pH could be
644 reconstructed by (i) solving the Mg/Ca dependency to temperature using Δ_{47} -derived
645 temperatures and (ii) correcting for salinity using either the salinity estimated from sea level
646 variations (Gray et al., 2019) or the salinity estimated from the combination of a thermometer
647 (Δ_{47} -temperature or TEX_{86} as in Leutert et al. (2020)) and $\delta^{18}\text{O}$ (to obtain the $\delta^{18}\text{O}_{\text{sw}}$).

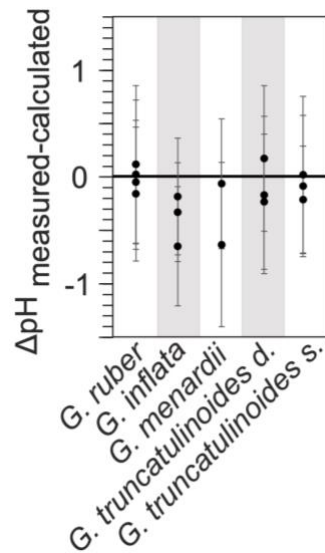
648 We tested such an approach with our core-top dataset. Firstly, $\delta^{18}\text{O}_{\text{sw}}$ was
649 reconstructed by pairing $\delta^{18}\text{O}$ and Δ_{47} and using the equation 1 (Kim and O'Neil, 1997). Then
650 salinity was reconstructed using modern salinity- $\delta^{18}\text{O}_{\text{sw}}$ relationships (section 2.4;
651 supplementary material Fig. S4, at our site locations). Finally, we used our raw Mg/Ca, the
652 estimated salinities and the clumped isotope temperatures to reconstruct pH values from the
653 equations of Gray and Evans (2019). The reconstructed pH is compared to the pH extracted
654 from the GLODAP 2020 data set (Olsen et al., 2020), by plotting their differences against the
655 different species (Fig. 6). For each species, the differences between estimated- and atlas-pH
656 (ΔpH) present a relatively good agreement, within the error bars, especially for *G. ruber* (Fig.
657 6). Part of the differences can be explained by the inaccurate assumptions regarding the depth
658 of life and the optimal developmental season of foraminifera species, thus leading to incorrect
659 pH being extracted from the atlases. Additionally, another limitation of this approach is the
660 salinity reconstruction that we applied. It requires to assume that, in the past, the regional
661 relationships between $\delta^{18}\text{O}_{\text{sw}}$ and salinity were the same as today. It is likely that in past
662 climates, regional changes of evaporation/precipitation and isotopic fractionation during

663 atmospheric transport of water vapor, lead to changes in the $\delta^{18}\text{O}_{\text{sw}}$ – salinity relationship. On
664 a global scale, these changes may have also altered the impact of ice sheet waxing/waning on
665 the seawater $\delta^{18}\text{O}_{\text{sw}}$ -salinity relationship. The extent and amount of sea ice may have also
666 decoupled this $\delta^{18}\text{O}_{\text{sw}}$ - salinity relationship (LeGrande and Schmidt, 2011). A direct application
667 of the $\delta^{18}\text{O}$ and Δ_{47} combination is therefore not straightforward and other methods of salinity
668 reconstruction should be used (Gray and Evans, 2019; Leutert et al., 2020).

669 Thus, despite the theoretical potential of the approach described above, it should be
670 noted that the uncertainties in pH are large (at 2SE in Fig. 6), making the application of this
671 approach challenging. It is important to note that these uncertainties are particularly large
672 with respect to expected pH changes in the geological past (see discussion below). The
673 uncertainties in the reconstructed pH range between 0.23 and 0.39, which is too high for
674 useful paleoceanographic reconstruction and conversion to atmospheric CO_2 concentration,
675 since it has been estimated that pH variations over G-IG cycles are on the order of 0.15 (e.g.
676 Hönisch and Hemming, 2005; Henehan et al., 2013), and by 0.2 units over the Miocene
677 (Leutert et al., 2020)). In terms of propagation of errors, the estimated pH uncertainties are
678 dominated by the uncertainties in the clumped isotope-derived temperatures. The Δ_{47}
679 uncertainties need to be reduced by measuring more replicates or by improvements in mass
680 spectrometry.

681 Further studies and technical improvements are needed to improve species-specific
682 equations and better understand the dependence of Mg/Ca on salinity and pH, and to reduce
683 the amount of material needed for Δ_{47} measurements and decrease temperature
684 uncertainties. It is also mandatory to improve our knowledge about past relationships
685 between $\delta^{18}\text{O}_{\text{sw}}$ and salinity. While we are not able yet to fully benefit from the combination
686 of Mg/Ca, $\delta^{18}\text{O}$ and Δ_{47} ratios, the systematic use of these proxies is nonetheless useful to
687 better understand these proxies, their biases and thus help their interpretations in
688 paleoceanographic studies. Pairing these paleothermometers with the boron isotope pH
689 proxy (e.g., Foster and Rae, 2016), which requires knowledge of temperature to calculate K_B
690 and pH, would allow for multiple independent constraints on past variations in pH and
691 temperature.

692



693

694 **Figure 6:** the difference for all the species from our dataset (excluding *O. universa*, *G. bulloides*
 695 and *N. pachyderma*) between the extracted pH from the atlas (GLOPAD 2020) and the
 696 reconstructed pH, using the equations from Gray and Evans (2019) with the raw Mg/Ca, the
 697 Δ_{47} -derived temperatures, and the combination of $\delta^{18}\text{O}$ and Δ_{47} -derived temperatures to
 698 reconstruct the $\delta^{18}\text{O}_{\text{sw}}$. The uncertainties correspond to the uncertainties associated with the
 699 reconstructed pH (2SE)

700

701 5. CONCLUSION

702

703 The Mg/Ca in 7 planktonic foraminifer species is affected by species, salinity and pH
 704 effects (Gray et al., 2018). A strong correlation exists between Δ_{47} and Mg/Ca data when the
 705 later are corrected for salinity and pH effects with the Δ_{47} values. The *G. bulloides*-Mg/Ca ratio
 706 appear to show anomalously high values compared to the Mg/Ca- Δ_{47} relationship observed
 707 for the other seven planktonic species. Another process(es) may affect Mg/Ca in this species
 708 and additional investigation is needed to better understand what controls high Mg/Ca we
 709 observe in this species.

710

711 The improved agreement observed between Mg/Ca- and Δ_{47} -derived temperatures
 712 when Mg/Ca values are corrected for salinity and pH suggests that the foraminiferal clumped
 713 isotopes may only be temperature dependent. As such, the combination of the foraminiferal
 714 Mg/Ca, $\delta^{18}\text{O}$ and Δ_{47} , could allow the temperature (Δ_{47} thermometer), salinity (by combining
 715 $\delta^{18}\text{O}$ and Δ_{47} , to reconstruct the $\delta^{18}\text{O}_{\text{sw}}$ and then, the salinity) and pH (the only remaining
 unknown) of the past seawater to be determined. However, at present, the application of this

716 later approach is nontrivial. In particular, the Δ_{47} -temperature uncertainties result in pH
717 uncertainties higher than the expected pH changes in the geological record. Furthermore, the
718 estimation of past salinity is also not straightforward. Finally, the species-specific Mg/Ca-pH
719 sensitivity (Gray and Evans, 2019) adds an additional complication when applying the
720 approach to extinct species.

721 This paper is also present an update of the foraminiferal clumped-isotope calibration
722 of Peral et al. (2018), that benefits from the latest methodological developments (data
723 processing and standardization) and can be directly applied to palaeoceanographic studies.

724

725 **References**

726

- 727 Anand P., Elderfield H. and Conte M. H. (2003) Calibration of Mg/Ca thermometry in
728 planktonic foraminifera from a sediment trap time series. *Paleoceanography*, 18(2).
- 729 Anderson, N. T., Kelson, J. R., Kele, S., Daëron, M., Bonifacie, M., Horita, J., T. J. Mackey, C. M.
730 John, T. Kluge, P. Petschnig, A. B. Jost, K. W. Huntinton, S. M. Bernasconi, Bergmann, K.
731 D. (2021). A unified clumped isotope thermometer calibration (0.5–1100° C) using
732 carbonate-based standardization. *Geophysical Research Letters*, e2020GL092069.
- 733 Barker S., Greaves M. and Elderfield H. (2003) A study of cleaning procedures used for
734 foraminiferal Mg/Ca paleothermometry. *Geochemistry, Geophys. Geosystems* 4, 1–20.
- 735 Bemis, B. E., Spero, H. J., Bijma, J., & Lea, D. W. (1998). Reevaluation of the oxygen isotopic
736 composition of planktonic foraminifera: Experimental results and revised
737 paleotemperature equations. *Paleoceanography*, 13(2), 150-160.
- 738 Bernasconi, S. M., Daëron, M., Bergmann, K. D., Bonifacie, M., Meckler, A. N., Affek, H. P.,
739 (n.d.). InterCarb: A community effort to improve inter-laboratory standardization of the
740 carbonate clumped isotope thermometer using carbonate standards. *Geochemistry,*
741 *Geophysics* and
742 *Geosystems*. <https://doi.org/10.1002/essoar.10504430.410.1002/essoar.10504430.3e>
743 [ms](https://doi.org/10.1002/essoar.10504430.3e)
- 744 Bernasconi S. M., Müller I. A., Bergmann K. D., Breitenbach S. F. M., Fernandez A., Hodell D.
745 A., Jaggi M., Meckler A. N., Millan I. and Ziegler M. (2018) Reducing uncertainties in
746 carbonate clumped isotope analysis through consistent 3 carbon- ate-based
747 standardization. *Geochem. Geophys, Geosyst*.
- 748 Boyle, E. and Keigwin, L. (1985). Comparison of Atlantic and Pacific Paleochemical Records for
749 the Last 215,000 Years - Changes in Deep Ocean Circulation and Chemical Inventories.
750 *Earth and Planetary Science Letters*, 76:135–150.
- 751 Brand W. A., Assonov S. S. and Coplen T. B. (2010) Correction for the 17O interference in
752 $\delta(13C)$ measurements when analyzing CO₂ with stable isotope mass spectrometry
753 (IUPAC Technical Report). *Pure Appl. Chem.* 82, 1719–1733. Available at:
754 [https://www.degruyter.com/view/j/pac.2010.82.issue-8/pac-rep-09-01-05/pac-](https://www.degruyter.com/view/j/pac.2010.82.issue-8/pac-rep-09-01-05/pac-rep-09-01-05.xml)
755 [rep-](https://www.degruyter.com/view/j/pac.2010.82.issue-8/pac-rep-09-01-05/pac-rep-09-01-05.xml)
[09-01-05.xml](https://www.degruyter.com/view/j/pac.2010.82.issue-8/pac-rep-09-01-05/pac-rep-09-01-05.xml).
- 756 Breitenbach S. F. M., Mleneck-Vautravers M. J., Grauel A.-L., Lo L., Bernasconi S. M., Müller I.
757 A., Rolfe J., Greaves M. and Hodell D. A. (2018) Coupled Mg/Ca and clumped isotope

758 analyses of foraminifera provide consistent water temperatures. *Geochim.*
759 *Cosmochim. Acta* 236, 283–296.

760 Daëron, M., Blamart, D., Peral, M., & Affek, H. P. (2016). Absolute isotopic abundance ratios
761 and the accuracy of $\Delta 47$ measurements. *Chemical Geology*, 442, 83–96.

762 Daëron, M., Drysdale, R. N., Peral, M., Huyghe, D., Blamart, D., Coplen, T. B., ... & Zanchetta,
763 G. (2019). Most Earth-surface calcites precipitate out of isotopic equilibrium. *Nature*
764 *communications*, 10(1), 1–7.

765 Daëron, M. (2021). Full propagation of analytical uncertainties in $\Delta 47$
766 measurements. *Geochemistry, Geophysics, Geosystems*, 22(5), e2020GC009592.

767 de Villiers S., Greaves M. and Elderfield H. (2002) An intensity ratio calibration method for the
768 accurate determination of Mg/Ca and Sr/Ca of marine carbonates by ICP- AES.
769 *Geochemistry, Geophys. Geosystems* 3, n/a-n/a. Available at:
770 <http://doi.wiley.com/10.1029/2001GC000169>.

771 Deuser, W. G., and E. H. Ross. 1989. Seasonally abundant planktonic foraminifera of the
772 Saragossa Sea: Succession, deep-water fluxes, isotopic compositions, and
773 paleoceanographic implications, *J. Foraminiferal Res.*, 19, 268–293

774 Eiler, J.M. (2007) “Clumped-isotope” geochemistry—the study of naturally-occurring, multiply-
775 substituted isotopologues. *Earth Planet. Sci. Lett.* 262, 309–327.

776 Eiler, J.M. (2011) Paleoclimate reconstruction using carbonate clumped isotope thermometry.
777 *Quat. Sci. Rev.* 30 (25–26), 3575–3588. [https://doi.org/10.1016/j.](https://doi.org/10.1016/j.quascirev.2011.09.001)
778 [quascirev.2011.09.001](https://doi.org/10.1016/j.quascirev.2011.09.001)

779 Elderfield H., Gansen G. (2000). Past temperature and $\delta^{18}\text{O}$ of surface ocean waters inferred
780 from foraminiferal Mg/Ca ratios. *Nature*, 405, pp. 422–445

781 Elderfield, H., Vautravers, M., & Cooper, M. (2002). The relationship between shell size and
782 Mg/Ca, Sr/Ca, $\delta^{18}\text{O}$, and $\delta^{13}\text{C}$ of species of planktonic foraminifera. *Geochemistry,*
783 *Geophysics, Geosystems*, 3(8), 1–13.

784 Elderfield H., Yu J., Anand P., Kiefer T. and Nyland B. (2006) Calibrations for benthic
785 foraminiferal Mg/Ca paleothermometry and the carbonate ion hypothesis. *Earth Planet.*
786 *Sci. Lett.* 250, 633–649.

787 Elderfield H., Greaves M., Barker S., Hall I. R., Tripathi A., Ferretti P., Crowhurst S., Booth L. and
788 Daunt C. (2010) A record of bottom water temperature and seawater $\delta^{18}\text{O}$ for the
789 Southern Ocean over the past 440 kyr based on Mg / Ca of benthic foraminiferal
790 *Uvigerina* spp. *Quat. Sci. Rev.* 29, 160–169. Available at:
791 <http://dx.doi.org/10.1016/j.quascirev.2009.07.013>.

792 Evans, D., Brierley, C., Raymo, M. E., Erez, J., & Müller, W. (2016). Planktic foraminifera shell
793 chemistry response to seawater chemistry: Pliocene–Pleistocene seawater Mg/Ca,
794 temperature and sea level change. *Earth and Planetary Science Letters*, 438, 139–148.

795 Evans, D., Sagoo, N., Renema, W., Cotton, L. J., Müller, W., Todd, J. A., ... & Affek, H. P. (2018).
796 Eocene greenhouse climate revealed by coupled clumped isotope-Mg/Ca
797 thermometry. *Proceedings of the National Academy of Sciences*, 115(6), 1174–1179.

798 Erez, J. (2003). The source of ions for biomineralization in foraminifera and their implications
799 for paleoceanographic proxies. *Reviews in mineralogy and geochemistry*, 54(1), 115–
800 149.

801 Fiebig, J., Daëron, M., Bernecker, M., Guo, W., Schneider, G., Boch, R., Bernasconi, S., Jautzy,
802 J., & Dietzel, M. (2021). Calibration of the dual clumped isotope thermometer for
803 carbonates. *Geochimica et Cosmochimica Acta*, 312, 235–256.

804 Foster, G. L., & Rae, J. W. (2016). Reconstructing ocean pH with boron isotopes in
805 foraminifera. *Annual Review of Earth and Planetary Sciences*, 44, 207-237.

806 Grauel A. L., Schmid T. W., Hu B., Bergami C., Capotondi L., Zhou L. and Bernasconi S. M. (2013)
807 Calibration and application of the “clumped isotope” thermometer to foraminifera for
808 high-resolution climate reconstructions. *Geochim. Cosmochim. Acta* 108, 125–140.
809 Available at: <http://dx.doi.org/10.1016/j.gca.2012.12.049>.

810 Gray, W. R., Weldeab, S., Lea, D. W., Rosenthal, Y., Gruber, N., Donner, B., & Fischer, G. (2018).
811 The effects of temperature, salinity, and the carbonate system on Mg/Ca in
812 Globigerinoides ruber (white): A global sediment trap calibration. *Earth and Planetary
813 Science Letters*, 482, 607–620. <https://doi.org/10.1016/j.epsl.2017.11.026>

814 Gray, W. R., & Evans, D. (2019). Nonthermal influences on Mg/Ca in planktonic foraminifera:
815 A review of culture studies and application to the last glacial
816 maximum. *Paleoceanography and Paleoclimatology*, 34(3), 306-315.

817 Hönisch, B., & Hemming, N. G. (2005). Surface ocean pH response to variations in pCO₂
818 through two full glacial cycles. *Earth and Planetary Science Letters*, 236(1-2), 305-314.

819 Henehan, M. J., Rae, J. W., Foster, G. L., Erez, J., Prentice, K. C., Kucera, M., ... & Elliott, T.
820 (2013). Calibration of the boron isotope proxy in the planktonic foraminifera
821 Globigerinoides ruber for use in palaeo-CO₂ reconstruction. *Earth and Planetary Science
822 Letters*, 364, 111-122.

823 Kim S.-T. and O’Neil J. R. (1997) Equilibrium and nonequilibrium oxygen isotope effects in
824 synthetic carbonates. *Geochim. Cosmochim. Acta* 61, 3461–3475. Available at:
825 <http://linkinghub.elsevier.com/retrieve/pii/S0016703797001695>.

826 Kisakürek, B., A. Eisenhauer, F. Böhm, D. Garbe-Schönberg, and J. Erez (2008), Controls on
827 shell Mg/Ca and Sr/Ca in cultured planktonic foraminiferan, Globigerinoides ruber
828 (white), *Earth Planet. Sci. Lett.*, 273, 260–269, doi:10.1016/j.epsl.2008.06.026.

829 Kissel C., Laj C., Mulder T., Wandres C. and Cremer M. (2009) The magnetic fraction: A tracer
830 of deep water circulation in the North Atlantic. *Earth Planet. Sci. Lett.* 288, 444–454.
831 <https://doi.org/10.1016/j.epsl.2009.10.005>.

832 Kissel C., Van Toer A., Laj C., Cortijo E. and Michel E. (2013) Variations in the strength of the
833 North Atlantic bottom water during Holocene. *Earth Planet. Sci. Lett.* 369, 248–259.

834 Lea, D., T. Mashiotta, and H. Spero (1999), Controls on magnesium and strontium uptake in
835 planktonic foraminifera determined by live culturing, *Geochim. Cosmochim. Acta*, 63,
836 2369–2379, doi:10.1016/S0016-7037(99)00197-0.

837 Lea DW (2014) Elemental and isotopic proxies of past ocean temperatures. *Treatise on
838 Geochemistry*, eds Holland HD, Turekian KK (Elsevier, Amsterdam), 2nd Ed, pp 373–397.

839 Lear, C. H., Rosenthal, Y., & Slowey, N. (2002). Benthic foraminiferal Mg/Ca-
840 paleothermometry: A revised core-top calibration. *Geochimica et Cosmochimica
841 Acta*, 66(19), 3375-3387.

842 LeGrande A. N. and Schmidt G. A. (2006) Global gridded data set of the oxygen isotopic
843 composition in seawater. *Geophys. Res. Lett.* 33, 1–5.

844 LeGrande, A. N., and Schmidt G. A. (2011), Water isotopologues as a quantitative paleosalinity
845 proxy, *Paleoceanography*, 26, PA3225, doi:10.1029/2010PA002043

846 Leutert, T. J., Auderset, A., Martínez-García, A., Modestou, S., & Meckler, A. N. (2020). Coupled
847 Southern Ocean cooling and Antarctic ice sheet expansion during the middle
848 Miocene. *Nature Geoscience*, 13(9), 634-639.

849 Marchitto, T. M., Bryan, S. P., Curry, W. B., & McCorkle, D. C. (2007). Mg/Ca temperature
850 calibration for the benthic foraminifer *Cibicidoides*
851 *pachyderma*. *Paleoceanography*, 22(1).

852 Marchitto T. M., Curry W. B., Lynch-Stieglitz J., Bryan S. P., Cobb K. M. and Lund D. C. (2014)
853 Improved oxygen isotope temperature calibrations for cosmopolitan benthic foraminifera.
854 *Geochim. Cosmochim. Acta* 130, 1–11. [https://doi.org/ 10.1016/j.gca.2013.12.034](https://doi.org/10.1016/j.gca.2013.12.034).

855 Mathien-Blard E. and Bassinot F. (2009) Salinity bias on the foraminifera Mg/Ca thermometry:
856 Correction procedure and implications for past ocean hydrographic reconstructions.
857 *Geochemistry, Geophys. Geosystems* 10.

858 Meckler A. N., Ziegler M., Millán M. I., Breitenbach S. F. M. and Bernasconi S. M. (2014) Long-
859 term performance of the Kiel carbonate device with a new correction scheme for
860 clumped isotope measurements. *Rapid Commun. Mass Spectrom.* 28, 1705–1715.

861 Meinicke, N., Ho, S. L., Hannisdal, B., Nürnberg, D., Tripathi, A., Schiebel, R., & Meckler, A. N.
862 (2020). A robust calibration of the clumped isotopes to temperature relationship for
863 foraminifers. *Geochimica et Cosmochimica Acta*, 270, 160-183.

864 Meinicke, N., Reimi, M. A., Ravelo, A. C., & Meckler, A. N. Coupled Mg/Ca and clumped isotope
865 measurements indicate lack of substantial mixed layer cooling in the Western Pacific
866 Warm Pool during the last~ 5 million years. *Paleoceanography and Paleoclimatology*,
867 e2020PA004115.

868 Mulitza, S., Boltovskoy, D., Donner, B., Meggers, H., Paul, A., Wefer, G. (2003) Temperature:
869 $\delta^{18}\text{O}$ relationships of planktonic foraminifera collected from surface waters.
870 *Palaeogeography, Palaeoclimatology, Palaeoecology*, 202(1–2), 143-152.
871 [https://doi.org/10.1016/S0031-0182\(03\)00633-3](https://doi.org/10.1016/S0031-0182(03)00633-3).

872 Nummerger, L., Hemleben, C., Hoffmann, R., Mackensen, A., Schulz, H., Wunderlich, J. M., &
873 Kucera, M. (2009). Habitats, abundance patterns and isotopic signals of morphotypes of
874 the planktonic foraminifer *Globigerinoides ruber* (d'Orbigny) in the eastern
875 Mediterranean Sea since the Marine Isotopic Stage 12. *Marine Micropaleontology*, 73(1-
876 2), 90-104.

877 Nürnberg, D., J. Bijma, and C. Hemleben (1996), Assessing the reliability of magnesium in
878 foraminiferal calcite as a proxy for water mass temperatures, *Geochim. Cosmochim.*
879 *Acta*, 60, 803–814, doi:10.1016/0016-7037(95)00446-7.

880 Olsen, A., Lange, N., Key, R M., Tanhua, T., Bittig, H C., Kozyr, A., Álvarez, M., Azetsu-Scott, K.,
881 Becker, S., Brown, P J., Carter, B R., da Cunha, L., Feely, R A., van Heuven, S., Hoppema,
882 M., Ishii, M., Jeansson, E., Jutterström, S., Landa, C S., Lauvset, S K., Michaelis, P., Murata,
883 A., Pérez, F F., Pfeil, B., Schirnack, C., Steinfeldt, R., Suzuki, T., Tilbrook, B., Velo, A.,
884 Wanninkhof, R., Woosley, R. J. (2020). An updated version of the global interior ocean
885 biogeochemical data product, GLODAPv2. 2020. *Earth System Science Data*, 12(4), 3653-
886 3678.

887 Pang, X., Bassinot, F., & Sepulcre, S. (2020). Cleaning method impact on the Mg/Ca of three
888 planktonic foraminifer species: A downcore study along a depth transect. *Chemical*
889 *Geology*, 549, 119690.

890 Oomori, T., Kaneshima, H., Maezato, Y., Kitano, Y., 1987. Distribution coefficient of Mg²⁺ ions
891 between calcite and solution at 10–50°C. *Marine Chemistry* 20, pp. 327-336.

892 Osborne, E. B., Umling, N. E., Bizimis, M., Buckley, W., Sadekov, A., Tappa, E., ... & Thunell, R.
893 C. (2020). A sediment trap evaluation of B/Ca as a carbonate system proxy in asymbiotic
894 and nondinoflagellate hosting planktonic foraminifera. *Paleoceanography and*
895 *Paleoclimatology*, 35(2), e2019PA003682.

896 Passey, B. H., & Henkes, G. A. (2012). Carbonate clumped isotope bond reordering and
897 geospeedometry. *Earth and Planetary Science Letters*, 351, 223-236.

898 Peral M., Daëron M., Blamart D., Bassinot F., Dewilde F., Smialkowski N., Isguder G., Jorissen
899 F., Kissel C., Michel E., Vázquez Riveiros, N. and Waelbroeck C. (2018) ScienceDirect
900 Updated calibration of the clumped isotope thermometer in planktonic and benthic
901 foraminifera. 239, 1–16.

902 Peral, M., Blamart, D., Bassinot, F., Daëron, M., Dewilde, F., Rebaubier, H., Nomade, S., Girone,
903 A., Marimo, M., Maiorano, P., & Ciaranfi, N. (2020). Changes in temperature and oxygen
904 isotopic composition of Mediterranean water during the Mid-Pleistocene transition in
905 the Montalbano Jonico section (southern Italy) using the clumped-isotope
906 thermometer. *Palaeogeography, Palaeoclimatology, Palaeoecology*, 544, 109603.

907 Petersen, S. V., Defliese, W.F., Saenger, C., Daëron, M., John, C. M., Huntington, K. W., Kelson,
908 J. R., Bernasconi, S. M., Colman, A. S., Kluge, T., Olack, G. A., Schauer, A. J., Bajnai, D.,
909 Bonifacie, M., Breitenbach, S. F. M., Fiebig, J., Fernandez, A. B., Henkes, G. A., Hodell, D.,
910 Katz, A., Kele, S., Lohmann, K. C., Passey, B. H., Peral, M., Petrizzo, D. A., Rosenheim, B.
911 E., Tripathi, A., Venturelli, R., Young, E. D., Wacker U., Winkelstern, I. Z. 2019. *Effects of*
912 *Improved ¹⁷O Correction on Inter-Laboratory Agreement in Clumped Isotope*
913 *Calibrations, Estimates of Mineral-Specific Offsets, and Acid Fractionation Factor*
914 *Temperature Dependence*. Special Issue of *Geochemistry, Geophysics, Geosystems*, 20,
915 3495 – 3519

916 Piasecki, A., Bernasconi, S. M., Grauel, A., Hannisdal, B., Ho, S. L., Leutert, T. J., et al.
917 (2019). Application of clumped isotope thermometry to benthic
918 foraminifera. *Geochemistry, Geophysics, Geosystems*,
919 2018GC007961. <https://doi.org/10.1029/2018GC007961>

920 Regenberg, M., Steph, S., Nürnberg, D., Tiedemann, R., & Garbe-Schönberg, D. (2009).
921 Calibrating Mg/Ca ratios of multiple planktonic foraminiferal species with $\delta^{18}\text{O}$ -
922 calcification temperatures: Paleothermometry for the upper water column. *Earth and*
923 *Planetary Science Letters*, 278(3-4), 324-336.

924 Rebotim, A., Voelker, A. H., Jonkers, L., Waniek, J. J., Meggers, H., Schiebel, R., ... & Kucera, M.
925 (2017). Factors controlling the depth habitat of planktonic foraminifera in the
926 subtropical eastern North Atlantic. *Biogeosciences*, 14(4), 827-859.

927 Retailleau, S., Schiebel, R., & Howa, H. (2011). Population dynamics of living planktic
928 foraminifers in the hemipelagic southeastern Bay of Biscay. *Marine*
929 *Micropaleontology*, 80(3-4), 89-100.

930 Roche, D.M., C. Waelbroeck, B. Metcalfe, T. Caley, 2018. FAME (v1. 0): a simple module to
931 simulate the effect of planktonic foraminifer species-specific habitat on their oxygen
932 isotopic content. *Geoscientific Model Development* 11(9), 3587-3603.

933 Rodríguez-Sanz, L., Bernasconi, S.M., Marino, G. *et al.* Author Correction: Penultimate
934 deglacial warming across the Mediterranean Sea revealed by clumped isotopes in
935 foraminifera. *Sci Rep* 11, 17511 (2021). <https://doi.org/10.1038/s41598-021-96895-3>

936 Rosenthal, Y., Boyle, E. A., & Slowey, N. (1997). Temperature control on the incorporation of
937 magnesium, strontium, fluorine, and cadmium into benthic foraminiferal shells from
938 Little Bahama Bank: Prospects for thermocline paleoceanography. *Geochimica et*
939 *Cosmochimica Acta*, 61(17), 3633-3643.

940 Schauble E. A., Ghosh P. and Eiler J. M. (2006) Preferential formation of ^{13}C - ^{18}O bonds in
941 carbonate minerals, estimated using first-principles lattice dynamics. *Geochim.*
942 *Cosmochim. Acta* 70, 2510–2529.

- 943 Shackleton N. (1967) Oxygen isotope analyses and Pleistocene temperatures re-assessed.
944 Nature 215, 15–17.
- 945 Shackleton N.J. (1974) Attainment of isotopic equilibrium between ocean water and
946 benthonic foraminifera genus *Uvigerina*: isotopic changes in the ocean during the last
947 glacial. Les méthodes quantitatives d'étude des variations du climat au cours du
948 Pleistocène, Gif-sur-Yvette. Colloque international du CNRS, 219, pp. 203-210
- 949 Spero H.J., Bijma J., Lea D.W., Bermis B.E. (1997) Effect of seawater carbonate concentration
950 on foraminiferal carbon and oxygen isotopes. *Nature*, 390, 497-500.
- 951 Spero H.J., Bijma J., Lea D.W., Russell, A.D. (1999) Deconvolving glacial ocean carbonate
952 chemistry from the planktonic foraminifera carbon isotope record.
953 F. Abrantes, A.C. Mix (Eds.), *Reconstructing Ocean History: A Window into the*
954 *Future*, Kluwer Academic/Plenum Publishers, New York, 329-342
- 955 Steinke, S., Chiu, H. Y., Yu, P. S., Shen, C. C., Löwemark, L., Mii, H. S., & Chen, M. T. (2005).
956 Mg/Ca ratios of two *Globigerinoides ruber* (white) morphotypes: Implications for
957 reconstructing past tropical/subtropical surface water conditions. *Geochemistry,*
958 *Geophysics, Geosystems*, 6(11).
- 959 Stewart, J. A., Christopher, S. J., Kucklick, J. R., Bordier, L., Chalk, T. B., Dapoigny, A., Douville,
960 E., Foster, G. L., Gray, W. R., Greenop, R., Gutjahr, M., Hemsing, F., Henehan, M. J.,
961 Holdship, P., Hsieh, Y., Kolevica, A., Lin, Y., Mawbey, E. M., Rae, J. W. B., Robinson, L. F.,
962 Shuttleworth, R., You, C., Zhang, S., & Day, R. D. (2021). NIST RM 8301 boron isotopes in
963 marine carbonate (simulated coral and foraminifera solutions): inter-laboratory $\delta^{11}\text{B}$
964 and trace element ratio value assignment. *Geostandards and Geoanalytical*
965 *Research*, 45(1), 77-96.
- 966 Stolper D. A. and Eiler J. M. (2016) Constraints on the formation and diagenesis of
967 phosphorites using carbonate clumped isotopes. *Geochim. Cosmochim. Acta* 181, 238–
968 259.
- 969 Tierney, J. E., Malevich, S. B., Gray, W., Vetter, L., & Thirumalai, K. (2019). Bayesian calibration
970 of the Mg/Ca paleothermometer in planktic foraminifera. *Paleoceanography and*
971 *Paleoclimatology*, 34, 2005–2030. <https://doi.org/10.1029/2019PA003744>
- 972 Tripathi A. K., Eagle R. A., Thiagarajan N., Gagnon A. C., Bauch H., Halloran P. R. and Eiler J. M.
973 (2010) ^{13}C - ^{18}O isotope signatures and “clumped isotope” thermometry in foraminifera
974 and coccoliths. *Geochim. Cosmochim. Acta* 74, 5697–5717. Available at:
975 <http://dx.doi.org/10.1016/j.gca.2010.07.006>.
- 976 Tripathi, A. K., Hill, P. S., Eagle, R. A., Mosenfelder, J. L., Tang, J., Schauble, E. A., ... & Henry, D.
977 (2015). Beyond temperature: Clumped isotope signatures in dissolved inorganic carbon
978 species and the influence of solution chemistry on carbonate mineral
979 composition. *Geochimica et Cosmochimica Acta*, 166, 344-371.
- 980 Urey, H.C., Lowenstam, H.A., Epstein, S. and McKinney, C.R. (1951): Measurements of
981 paleotemperatures and temperatures of the Upper Cretaceous of England, Denmark
982 and the southeastern United States. *Bull. Geo. Soc. of Am.*, 62: 399-416.
- 983 Vázquez Riveiros N., Govin A., Waelbroeck C., Mackensen A., Michel E., Moreira S., Bouinot T.,
984 Caillon N., Orgun A. and Brandon M. (2016) Mg/Ca thermometry in planktic foraminifera:
985 improving paleotemperature estimations for *G. bulloides* and *N. pachyderma* left.
986 *Geochem. Geophys. Geosy.* 17, 1249– 1264. <https://doi.org/10.1002/2015GC006234>
- 987 Watkins, J. M., & Hunt, J. D. (2015). A process-based model for non-equilibrium clumped
988 isotope effects in carbonates. *Earth and Planetary Science Letters*, 432, 152-165.

989 Whitaker J., Khrulev C., Huard D., Paulik C., Hoyer S., Mohr F. A., Marquardt C., Couwenberg
990 B., Bohnet M., Brett M., Hetland R., Korenčiak M., Onu K., Helmus J. J., Hamman J.,
991 Barna A., Koziol B., Kluyver T., May R., Smrekar J., Barker C., Davar G., Cournapeau
992 D., da Silva D., Gohlke C., Kinoshita B. P. (2019). Unidata/netcdf4-python: version
993 1.4.3.2 release (v1.4.3.2). Zenodo. <https://doi.org/10.5281/zenodo.2592291>
994 Yu, J.M., Day, J., Greaves, M., Elderfield, H., 2005. Determination of multiple element/calcium
995 ratios in foraminiferal calcite by quadrupole ICP-MS. *Geochem. Geophys. Geosyst.* 6,
996 Q08P01. doi:10.1029/2005GC000964.
997 Zeebe R.E. (1999). An explanation of the effect of seawater carbonate concentration on
998 foraminiferal oxygen isotopes. *Geochim. Cosmochim. Acta*, 63, 2001-2007.
999 Zweng, M.M, J.R. Reagan, J.I. Antonov, R.A. Locarnini, A.V. Mishonov, T.P. Boyer, H.E. Garcia,
1000 O.K. Baranova, D.R. Johnson, D.Seidov, M.M. Biddle, 2013. *World Ocean Atlas 2013,*
1001 *Volume 2: Salinity.* S. Levitus, Ed., A. Mishonov Technical Ed.; NOAA Atlas NESDIS 74, 39
1002 pp.

1003 **Author contributions**

1004 MP and FB have designed the study. MP wrote the manuscript, and all co-authors help in the
1005 writing. MD provided the python code to reprocess the clumped-isotope calibration. FB, DB,
1006 MD and WG provided assistance in the interpretation of the clumped-isotope and/or Mg/Ca
1007 data. JB, FJ, CK, EM and CW helped in the selection of the marine sediment cores and
1008 foraminifer species. MP hand-picked the foraminiferal samples. MP and HR cleaned the
1009 samples for the Mg/Ca measurements and HR and WG performed the Mg/Ca measurements.

1010

1011 **Acknowledgements**

1012 All authors thank the editor for his patience in the lengthy process of reviewing this article and
1013 the 3 anonymous reviewers for their really useful comments that significantly improve the
1014 manuscript. MP thanks the CEA for the financially support during her 3-years PhD fellowship
1015 2015-2018.

Table 1: Core top locations and water depth with species considered in this study and chronological.

Cores	Latitude (°)	Longitude (°)	Water depth (m)	Species	Core-top cal. yrs BP (95% CL)	References
MOCOSDSt1	73.04	-11.93	1839	<i>Cibicides wuellerstorfi</i> ; <i>N. pachyderma s</i>	6317 (+150/-94) *	(1)
MD04-2720	-49.13	71.36	750	<i>N. pachyderma d</i>	n.a.	
MD12-3401	-44.69	80.4	3445	<i>G. bulloides</i>	< 4000 **	(2)
MD95-2014	60.59	-22.08	2397	<i>G. bulloides</i>	715 (+94/-149) *	(1)
MD08-3182Q	52.71	-35.94	1355	<i>N. pachyderma s</i> ; <i>G. bulloides</i>	500 (+40/-53) *	(3)
MD03-2680Q	61.06	-24.55	1812	<i>N. pachyderma d</i>	402	(4)
2FPA1	43.67	-2.00	664	<i>Uvigerina mediterranea</i>	< 4000 ***	(1)
SU90I-03	40.05	-30	2475	<i>G. bulloides</i>	2013 (+125/-120) *	(1)
MD08-3179Q	37.86	-30.3	2036	<i>G. ruber</i> ; <i>G. inflata</i> ; <i>G. truncatulinoides s</i> ; <i>G. truncatulinoides d</i>	4403 (+153/-121) *	(1)
MD12-3426Q	19.73	114.61	3630	<i>G. menardii</i> ; <i>O. universa</i>	1755 (+159/-139) *	(1)
MD00-2360	-20.08	112.67	980	<i>G. menardii</i> ; <i>O. universa</i> ; <i>G. ruber</i>	3622 (+135/-137) *	(1)
MD02-2577Q	28.84	-86.67	4076	<i>G. menardii</i> ; <i>O. universa</i> ; <i>G. ruber</i>	1107 (+110/-105) *	(1)

* Age determined by radiocarbon dating

** Age determined by stratigraphic control

*** Age determined by presence of Rose Bengal

(1) Peral et al., 2018; (2) Vazquez Riveiros et al., 2016; (3) Kissel et al., 2013 and (4) Kissel et al., 2009

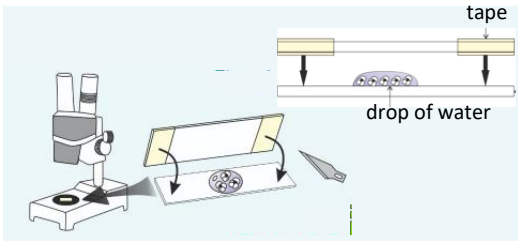
Table 2: Summary of the main results used in this study. The samples/species are represented with the optimal size fraction. The raw Mg/Ca values are presented, as well as the $\delta^{18}\text{O}_c$ and the recalculated Δ_{47} values with their associated uncertainties at 1SE. We also present the corrected Mg/Ca values for salinity and pH. Seawater salinity from WOA and pH from GLODAP 2020 (Olsen et al., 2020), are reported.

Core	Species	Optimal Size	$\delta^{18}\text{O}_c$ VPDB (‰)	SE	Δ_{47} (‰)	SE	Mg/Ca raw	SE	Mg/Ca corrected	SE	pH reconstructed	SE
MD08-3182	<i>G. bulloides</i>	250-315	1.77	0.1	0.6489	0.0074	2.10	0.006	2.24	0.309	7.941	0.27
MD08-3182	<i>G. bulloides</i>	315-355	1.87	0.1	0.665	0.0074	2.06	0.006	2.20	0.300	7.571	0.28
MD12-3401	<i>G. bulloides</i>	250-315	2.04	0.1	0.6626	0.0075	1.45	0.006	1.64	0.144	8.041	0.23
MD95-2014	<i>G. bulloides</i>	315-355	2.13	0.1	0.6492	0.0074	4.69	0.006	4.86	0.211	7.044	0.39
SU90-03	<i>G. bulloides</i>	250-315	1.59	0.1	0.6429	0.0063	3.30	0.006	3.44	0.427	7.570	0.30
MD08-3179	<i>G. inflata</i>	355-400	1.19	0.1	0.6286	0.0074	2.03	0.008	2.10	0.328	8.283	0.31
MD08-3179	<i>G. inflata</i>	400-450	1.08	0.1	0.6219	0.0073	1.68	0.008	1.76	0.339	8.747	0.29
MD08-3179	<i>G. inflata</i>	450-500	1.24	0.1	0.6247	0.0085	2.00	0.008	2.08	0.323	8.429	0.35
MD00-2360	<i>G. menardi menardi</i>	355-400	-0.37	0.1	0.5977	0.0075	2.85	0.004	3.15	0.354	8.741	0.37
MD00-2360	<i>G. menardi menardi</i>	400-450	-0.29	0.1	0.619	0.0074	2.55	0.004	2.84	0.346	8.170	0.34
MD00-2360	<i>G. ruber</i>	250-315	-1.76	0.1	0.5917	0.0058	4.34	0.008	4.88	0.643	8.262	0.32
MD02-2577	<i>G. ruber</i>	250-315	-1.33	0.1	0.5959	0.0073	4.59	0.008	4.71	0.813	8.099	0.37
MD02-2577	<i>G. ruber</i>	315-355	-1.46	0.1	0.5977	0.0073	4.63	0.008	4.75	0.847	8.029	0.37
MD08-3179	<i>G. ruber</i>	250-315	-0.08	0.1	0.6167	0.0073	3.21	0.008	3.37	0.597	7.988	0.33
MD08-3179	<i>G. truncatulinoides (d.)</i>	355-400	1.05	0.1	0.6424	0.0074	1.97	0.006	2.05	0.345	7.926	0.25
MD08-3179	<i>G. truncatulinoides (d.)</i>	400-450	1.14	0.1	0.6251	0.0074	2.09	0.006	2.16	0.336	8.331	0.34
MD08-3179	<i>G. truncatulinoides (d.)</i>	450-500	1.07	0.1	0.6278	0.0074	2.06	0.006	2.14	0.342	8.268	0.33
MD08-3179	<i>G. truncatulinoides (s.)</i>	355-400	1.08	0.1	0.638	0.0074	1.91	0.006	1.99	0.341	8.080	0.28
MD08-3179	<i>G. truncatulinoides (s.)</i>	400-450	1.07	0.1	0.6343	0.0074	1.90	0.006	1.98	0.342	8.184	0.30
MD08-3179	<i>G. truncatulinoides (s.)</i>	450-500	1.17	0.1	0.6342	0.0074	1.72	0.006	1.79	0.332	8.312	0.31
MD03-2680	<i>N. pachyderma (d.)</i>	200-250	1.73	0.1	0.647	0.0074	1.16	0.008	1.184	0.008		
MD04-2720	<i>N. pachyderma (d.)</i>	200-250	3.24	0.1	0.676	0.0075	0.76	0.008	0.87	0.008		
MD08-3182	<i>N. pachyderma (s.)</i>	200-250	1.76	0.1	0.6504	0.0074	1.09	0.006	1.17	0.006		
MOCOSD	<i>N. pachyderma (s.)</i>	200-250	2.86	0.1	0.6678	0.0074	0.90	0.006	1.15	0.006		

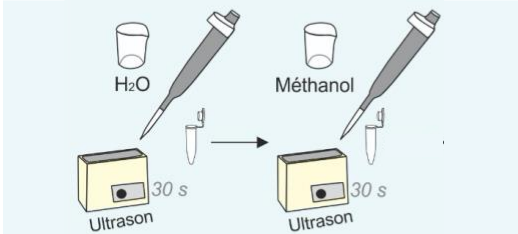
1 **Table 3:** Summary of all the Mg/Ca calibration used in this study: mono-specific species
 2 calibrations, calibration with salinity and pH corrections and the salinity and pH corrected
 3 multi-species calibration

Recalculated multi-species calibration from Anand et al., 2003					
Mg/Ca = B*exp(A*T)					
		Values	SE		
	A	0.0913	0.003		Recalculated in this study
	B	0.6109	0.002		
Mono-specific calibrations					
Mg/Ca = B*exp(A*T)					
		Values	SE	Size fraction	
<i>G. menardii</i>	A	0.091	0.012	355-400	Regenberg et al., 2009
	B	0.36	0.31		
<i>O. universa</i>	A	0.085	0.002	NA	Lea et al., 1999
	B	1.38	0.05		
	A	0.09		350-500	
	B	0.595	0.042		
<i>G. ruber</i>	A	0.09		250-350	Anand et al., 2003
	B	0.449	0.006		
	A	0.09		350-500	
	B	0.395	0.009		
<i>N. pachyderma s</i>	A	0.084	0.006	200-250	Vasquez Riveiros et al., 2016
	B	0.58	0.084		
<i>G. inflata</i>	A	0.09		350-500	
	B	0.299	0.005		
<i>G. truncatulinoides d.</i>	A	0.09		350-500	Anand et al., 2003
	B	0.359	0.008		
<i>G. truncatulinoides s.</i>	A	0.09		350-500	
	B	0.359	0.008		
<i>G. bulloides</i>	A	0.081	0.005	250-315	Elderfield and Ganssen. 2000 North Atlantic
	B	0.81	0.04		
	A	0.061	0.005	250-315	Elderfield and Ganssen. 2000 Southern Ocean
	B	0.996	0.038		
Mono-specific calibrations with SSS and pH corrections					
Mg/Ca=exp(A*(S - B) + C*T + D*(pH - E) + F					
		Values	SE		
<i>G. ruber</i>	A	0.036	0.006		
	B	35			
	C	0.061	0.005		
	D	-0.87	0.1		
	E	8	0		
	F	0.03	0.03		
<i>G. bulloides</i>	A	0.036	0.006		
	B	35			
	C	0.061	0.005		
	D	-0.88	0.12		
	E	8	0		
	F	0.21	0.04		Gray and Evans. 2019
<i>O. universa</i>	A	0.036	0.006		
	B	35			
	C	0.061	0.005		
	D	-0.51	0.11		
	E	8	0		
	F	0.77	0.48		
Multi-species	A	0.036	0.006		
	B	35			
	C	0.061	0.005		
	D	-0.73	0.07		
	E	8	0		
	F	0			

Step 1



Step 2



Step 3



Cleaning protocol for clumped isotope in foraminifera

Step 1: Crush the foraminifera

Gently crush foraminifera between two glass slides to open all chambers

Step 2: remove clay

Add milliQ water
Remove the water
Ultrasonic bath for 30s
Repeat 3 times or more until water remains clear and colourless

Add methanol
Ultrasonic bath for 30s
Remove the methanol
Repeat 2 time or more until the methanol remains clear and colourless

Remove the maximum of the methanol

Step 3: Dry

Dry at room temperature under a fume hood. Microtubes should be open but covered with aluminum foil to avoid dust contaminants

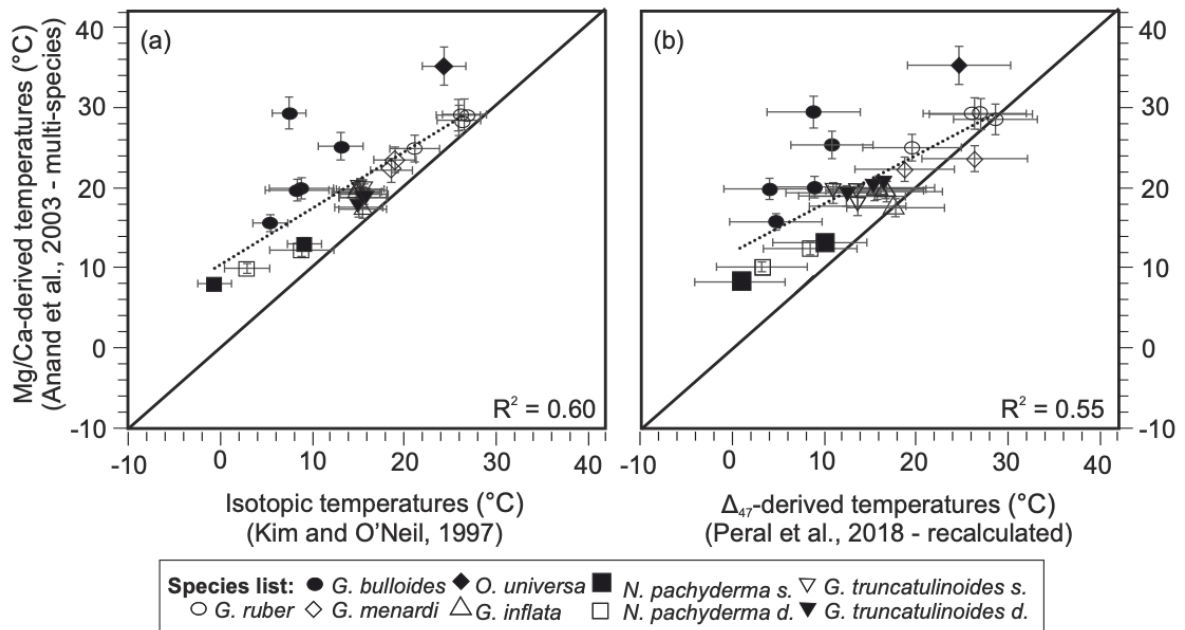
Equipment:

Microtubes, gloves, fume hood, microscope, 4 beaker (for water & dirty water and for methanol & dirty methanol), pipette and pipette tip (change for each sample or each step)

4
5
6

Figure S1: summary of the cleaning protocol steps for clumped isotope in foraminifera

7



8

9 **Figure S2:** reconstructed Mg/Ca temperatures using the original multi-species calibration of

10 Anand et al. (2003) compared to reconstructed $\delta^{18}\text{O}$ temperatures, using Kim and O'Neil

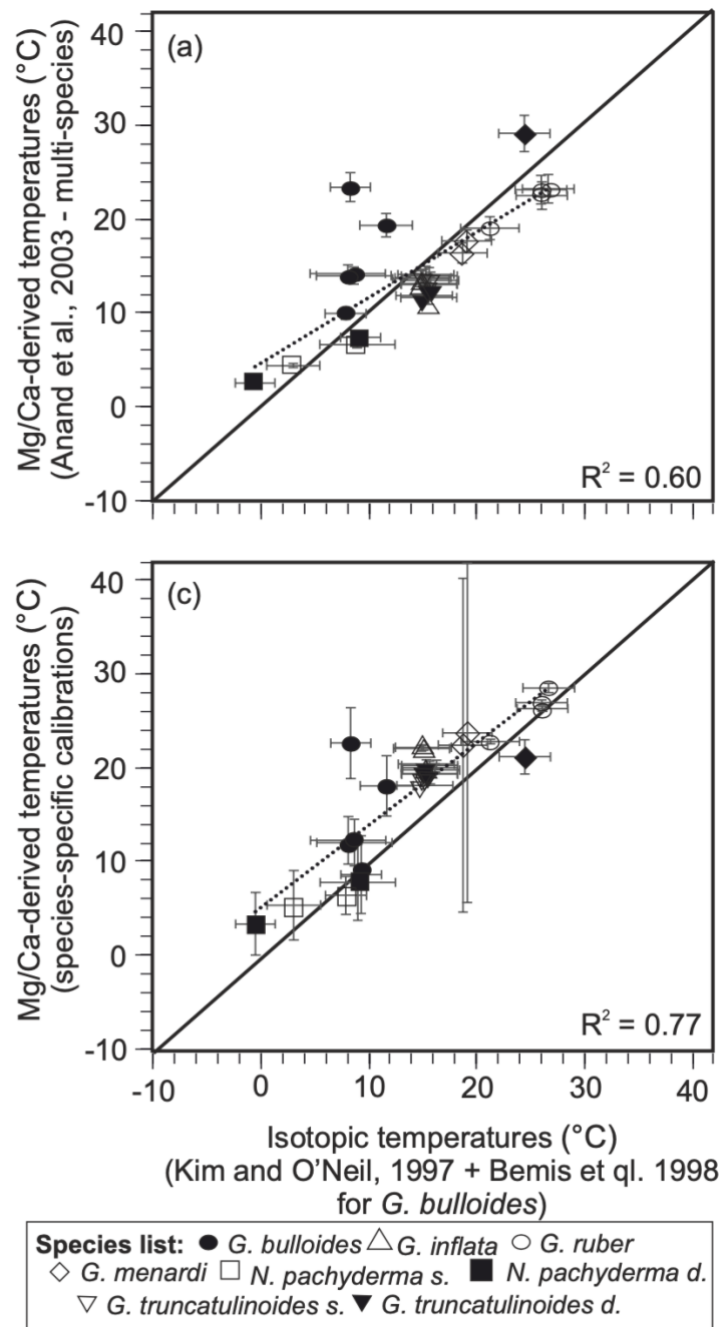
11 (1997) (a) and Δ_{47} -derived temperatures, using recalculated Peral et al. (2018) (b) for 9 planktic

12 foraminifera. The linear regressions are the dotted black lines, a line 1:1 is in black, and the

13 uncertainties are at 2 SE. The Mg/Ca-derived temperatures are systematically higher than the

14 isotopic-derived temperatures.

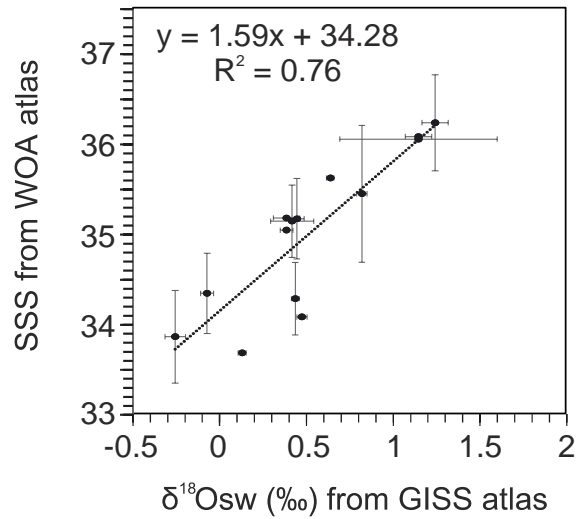
15



16

17 **Figure S3:** reconstructed Mg/Ca temperatures using the recalculated multi-species calibration
 18 of Anand et al. (2003) compared to reconstructed $\delta^{18}\text{O}$ temperatures, using Kim and O'Neil
 19 (1997) (a) and reconstructed Mg/Ca derived temperatures using the most adequate mono-
 20 specific calibrations compared to reconstructed $\delta^{18}\text{O}$ temperatures, using Kim and O'Neil
 21 (1997) and Bemis et al. (1998) calibration for *G. bulloides* (b). The linear regressions are the
 22 dotted black lines, the 1:1 line is the black solid line, and the uncertainties are at 2 SE.

23



24
 25 **Figure S4:** relationship between the seawater salinity from WOA 13 and the $\delta^{18}\text{O}$ of the
 26 seawater from GISS atlas for all our samples defined as core/species. For benthic foraminifera
 27 we used the available bottom data and planktonic foraminifera we integrated data withing
 28 the column water corresponding to the known living depths of each specie (see details in Peral
 29 et al., 2018). The linear regressions are the dotted black lines, a line 1:1 is in black, and the
 30 uncertainties are at 2 SE.
 31

32 **Figure 1:** Map of core-top location used in this study, with the mean annual SST from WOA13

33

34 **Figure 2:** Comparison of temperature estimates obtained on 9 planktonic species. Top panels:

35 reconstructed Mg/Ca temperatures using the recalculated multi-species calibration of Anand

36 et al. (2003) compared to reconstructed $\delta^{18}\text{O}$ temperatures, using Kim and O'Neil (1997) (a)

37 and Δ_{47} -derived temperatures, using recalculated Peral et al. (2018) (b). Bottom panel:

38 reconstructed Mg/Ca derived temperatures using the most adequate mono-specific

39 calibrations compared to reconstructed $\delta^{18}\text{O}$ temperatures, using Kim and O'Neil (1997) (c)

40 and Δ_{47} -derived temperatures, using recalculated Peral et al. (2018) calibration (d). Dotted

41 black lines are linear regressions, the black solid lines are the 1:1 line. Uncertainties are at 2SE.

42

43 **Figure 3:** Comparison of our recalculated foraminiferal Δ_{47} values with raw Mg/Ca values

44 (uncorrected) (a), with corrected Mg/Ca for salinity only (b), and with corrected Mg/Ca for

45 salinity and pH (c). The Mg/Ca values are corrected using the equations from Gray and Evans

46 (2019), the salinity and pH from the atlas and the oxygen isotopic temperatures. The red

47 dotted logarithmic regressions are plotted for all the plots, including *G. bulloides* and the black

48 regressions are without *G. bulloides*. All the uncertainties are at 2SE.

49

50 **Figure 4:** Recalculated Δ_{47} values (mean and 2SE) compared to oxygen isotopic temperatures

51 (mean and 2SE) obtained with Kim and O'Neil (1997) for planktonic (circle) and benthic

52 (square) foraminifera samples, combining all size fractions (modified from Peral et al., 2018).

53 The new calibration regression corresponds to the black line (Peral et al., 2018 recalculated).

54 The recalculated foraminiferal calibration is compared to the slow-growing calcite from

55 Laghetto Basso and Devils Hole (from Anderson et al., 2021) and to calibrations of Anderson

56 et al. (2021) and Fiebig et al. (2021)

57

58 **Figure 5:** Mg/Ca-derived temperatures using mono-species calibrations, compared to the Δ_{47} -

59 derived temperatures using the recalculated Peral et al. (2018) calibration (a) and the Mg/Ca-

60 derived temperatures using the corrected Mg/Ca mono-species calibrations for salinity and

61 pH compared to the Δ_{47} -derived temperatures using the recalculated Peral et al. (2018)

62 calibration (b). The dotted linear regression, excluding *O. universa* and *G. bulloides*, is plotted.

63 A line 1:1 is plotted in black; uncertainties are at 2 SE.

64

65 **Figure 6:** the difference for all the species from our dataset (excluding *O. universa*, *G. bulloides*
66 and *N. pachyderma*) between the extracted pH from the atlas (GLOPAD 2020) and the
67 reconstructed pH, using the equations from Gray and Evans (2019) with the raw Mg/Ca, the
68 Δ_{47} -derived temperatures, and the combination of $\delta^{18}\text{O}$ and Δ_{47} -derived temperatures to
69 reconstruct the $\delta^{18}\text{O}_{\text{sw}}$. The uncertainties correspond to the uncertainties associated with the
70 reconstructed pH (2SE)